

## Various nuclear structures in $^{140}\text{Xe}$ studied by $\beta$ decay of ground and isomeric states in $^{140}\text{I}$

A. Yagi,<sup>1,2</sup> A. Odahara ,<sup>1,\*</sup> H. Nishibata,<sup>1,2,3</sup> R. Lozeva,<sup>4,5</sup> C.-B. Moon,<sup>6,7</sup> S. Nishimura,<sup>2</sup> K. Yoshida,<sup>8</sup> N. Yoshinaga,<sup>9</sup> C. Watanabe,<sup>9</sup> K. Higashiyama,<sup>10</sup> T. Shimoda,<sup>1</sup> R. Daido,<sup>1,2</sup> Y. Fang,<sup>1,2</sup> P. S. Lee,<sup>11,2,12</sup> B. Moon,<sup>13,2,7</sup> P. Doornenbal,<sup>2</sup> G. Lorusso,<sup>2</sup> P.-A. Söderström,<sup>2,14</sup> T. Sumikama,<sup>2</sup> H. Watanabe,<sup>15</sup> T. Isobe,<sup>2</sup> H. Baba,<sup>2</sup> H. Sakurai,<sup>16,2</sup> F. Browne,<sup>17,2</sup> Z. Patel,<sup>18,2</sup> S. Rice,<sup>18,2</sup> L. Sinclair,<sup>19,2</sup> J. Wu,<sup>20,2</sup> Z. Y. Xu,<sup>16</sup> R. Yokoyama,<sup>21</sup> T. Kubo,<sup>2</sup> N. Inabe,<sup>2</sup> H. Suzuki,<sup>2</sup> N. Fukuda,<sup>2</sup> D. Kameda,<sup>2</sup> H. Takeda,<sup>2</sup> D. S. Ahn,<sup>2,7</sup> Y. Shimizu,<sup>2</sup> D. Murai,<sup>22</sup> F. L. Bello Garrote,<sup>23</sup> J.-M. Daugas,<sup>24</sup> F. Didierjean,<sup>4</sup> E. Ideguchi,<sup>25</sup> S. Iimura,<sup>1,2</sup> T. Ishigaki,<sup>1,2</sup> H. S. Jung,<sup>26</sup> T. Komatsubara,<sup>27</sup> Y. K. Kwon,<sup>27</sup> C. S. Lee,<sup>11</sup> S. Morimoto,<sup>1,2</sup> M. Niikura,<sup>16</sup> I. Nishizuka,<sup>28</sup> and K. Tshoo<sup>27</sup>

<sup>1</sup>*Department of Physics, Osaka University, Osaka 560-0043, Japan*

<sup>2</sup>*RIKEN, Wako, Saitama 351-0198, Japan*

<sup>3</sup>*Department of Physics, Kyushu University, Fukuoka 819-0395, Japan*

<sup>4</sup>*IPHC, CNRS, IN2P3, and University of Strasbourg, F-67037 Strasbourg Cedex 2, France*

<sup>5</sup>*Université Paris-Saclay, IJCLab, CNRS/IN2P3, F-91405 Orsay, France*

<sup>6</sup>*Department of Display Engineering, Hoseo University, Chung-Nam 336-795, Republic of Korea*

<sup>7</sup>*Center for Exotic Nuclear Studies, Institute for Basic Science, Daejeon 34126, Republic of Korea*

<sup>8</sup>*Department of Physics, Kyoto University, Kyoto 606-8502, Japan*

<sup>9</sup>*Department of Physics, Saitama University, Saitama City 338-8570, Japan*

<sup>10</sup>*Department of Physics, Chiba Institute of Technology, Chiba 275-0023, Japan*

<sup>11</sup>*Department of Physics, Chung-Ang University, Seoul 156-756, Republic of Korea*

<sup>12</sup>*Korea Multi-purpose Accelerator Complex, Korea Atomic Energy Research Institute, Mirae-ro 181, Gyeongju-si 38180, Republic of Korea*

<sup>13</sup>*Department of Physics, Korea University, Seoul 02841, Republic of Korea*

<sup>14</sup>*Extreme Light Infrastructure-Nuclear Physics (ELI-NP)/Horia Hulubei National Institute for Physics and Nuclear Engineering (IFIN-HH), Str. Reactorului 30, Bucharest-Măgurele 077125, Romania*

<sup>15</sup>*School of Physics and Nuclear Energy Engineering, Beihang University, Beijing 100191, China*

<sup>16</sup>*Department of Physics, University of Tokyo, Hongo, Tokyo 113-0033, Japan*

<sup>17</sup>*School of Computing, Engineering and Mathematics, University of Brighton, Brighton BN2 4JG, United Kingdom*

<sup>18</sup>*Department of Physics, University of Surrey, Guildford GU2 7XH, United Kingdom*

<sup>19</sup>*Department of Physics, University of York, Heslington, York YO10 5DD, United Kingdom*

<sup>20</sup>*School of Physics and State Key Laboratory of Nuclear Physics and Technology, Peking University, Beijing 100871, China*

<sup>21</sup>*CNS, University of Tokyo, 2-1 Hirosawa, Wako, Saitama 351-0198, Japan*

<sup>22</sup>*Department of Physics, Rikkyo University, Toshima, Tokyo 171-8501, Japan*

<sup>23</sup>*Department of Physics, University of Oslo, N-0316, Oslo, Norway*

<sup>24</sup>*CEA, DAM, DIF, F-91297 Arpaçon Cedex, France*

<sup>25</sup>*RCNP, Osaka University, Ibaraki, Osaka 567-0047, Japan*

<sup>26</sup>*Department of Physics, University of Notre Dame, Indiana 46556, USA*

<sup>27</sup>*Rare Isotope Science Project, Institute for Basic Science, Daejeon 305-811, Republic of Korea*

<sup>28</sup>*Department of Physics, Tohoku University, Miyagi 980-8578, Japan*



(Received 15 January 2022; accepted 1 April 2022; published 25 April 2022)

Structure of the neutron-rich  $N = 86$  isotope  $^{140}\text{Xe}$ , located northeast of a doubly-magic nucleus  $^{132}\text{Sn}$ , is investigated by  $\beta$ - $\gamma$  spectroscopy. Two  $\beta$ -decay isomers in  $^{140}\text{I}$  are newly found in the study of two different  $\beta$  decays of  $^{140}\text{I}$  which were produced by two reactions (i) direct in-flight fission at a primary target and (ii)  $\beta$  decay of  $^{140}\text{Te}$  at an active stopper. Half-lives of the  $\beta$  decays of the ground state, the low-spin isomer, and the high-spin isomer are determined to be 0.38(2), 0.91(5), and 0.47(4) s, respectively. Decay schemes of the  $\beta$  decay of the high-spin isomer and of the mixed  $\beta$  decays of the ground state and the low-spin isomer in  $^{140}\text{I}$  to  $^{140}\text{Xe}$  are constructed using the information on  $\gamma$ -ray coincidence relation and  $\gamma$ -ray intensity. Nuclear structures of the low-lying states in  $^{140}\text{Xe}$  and  $^{140}\text{I}$  are discussed by comparing the experimental results to two theoretical calculations based on a large-scale shell model and the deformed Skyrme Hartree-Fock-Bogoliubov plus deformed quasiparticle-random-phase approximation. Possible candidates for (quasi-) $\gamma$ -band members of

\* odahara@phys.sci.osaka-u.ac.jp

$2^+$  and  $4^+$  states and the octupole collective  $1^-$  state are proposed in  $^{140}\text{Xe}$ . Increase of quadrupole, triaxial, and octupole collectivities is discussed with the increase of neutron and proton numbers.

DOI: [10.1103/PhysRevC.105.044325](https://doi.org/10.1103/PhysRevC.105.044325)

## I. INTRODUCTION

Nuclear-shape transition studied with the increase of neutron and/or proton numbers is one of the most important subjects to disentangle competition between single-particle and collective modes in the finite quantum many-body system. Nuclei with neutron and/or proton numbers close to magic numbers are well known to have spherical shape and their nuclear structure is well described by the spherical single-particle model. However, nuclei with proton and neutron Fermi levels at the mid-shells between magic numbers are well known to have prolate dominating deformed shape and their structure is well described by the collective model. Nuclei in the transitional mass region (between spherical and deformed mass regions) are expected to exhibit coexistence with various shapes and motions due to the softness of nuclear potential. In this work, neutron-rich nuclei with  $A \sim 140$  in the transitional mass region between a doubly-magic nucleus  $^{132}\text{Sn}$  with spherical shape and well-known deformed nuclei with  $N = 90\text{--}100$  are studied. In this mass region, a more complex nuclear structure is expected to appear, because octupole vibration and octupole deformation were discussed and reported in the nuclei  $^{144}\text{Ba}$  ( $N = 88$ ) [1] and  $^{146}\text{Ba}$  ( $N = 90$ ) [2]. In this work, we focus on the nuclear structure of the transitional neutron-rich nucleus  $^{140}\text{Xe}$  ( $Z = 54$ ,  $N = 86$ ), which has four protons and four neutrons coupled to the doubly-magic  $^{132}\text{Sn}$  ( $Z = 50$ ,  $N = 82$ ) core.

The level structure of this  $^{140}\text{Xe}$  nucleus was reported in studies for experiments of spontaneous fission of  $^{248}\text{Cm}$  [3–5] and  $^{252}\text{Cf}$  [6–13] as well as thermal neutron-induced fission of  $^{235}\text{U}$  [14,15] and  $^{241}\text{Pu}$  [15]. Low-lying states were studied by  $\beta$  decay of  $^{140}\text{I}$  to  $^{140}\text{Xe}$  at the OSIRIS ISOL facility and a partial decay scheme was reported [16]. Quadrupole collectivity in  $^{140}\text{Xe}$  was discussed from half-lives of excited  $2_1^+$  and  $4_1^+$  levels populated by the  $\beta$  decay of  $^{140}\text{I}$  and by the thermal neutron-induced fission of  $^{235}\text{U}$  and  $^{241}\text{Pu}$  as well as the  $B(E2; 0_1^+ \rightarrow 2_1^+)$  value obtained in Coulomb excitation [17]. These half-lives and  $B(E2)$  values suggest vibrational nature and the extracted quadrupole-deformation parameter was reported to be 0.146(3) [16]. The reported  $g$  factor of the  $2^+$  state obtained by the correlation attenuation in randomly oriented magnetic fields in the spontaneous fission experiment of  $^{252}\text{Cf}$  [13] was reproduced by theoretical calculations on an IBM-2 model, indicating vibrational collectivity. The octupole band in  $^{140}\text{Xe}$  was found in the  $\beta$  decay of  $^{140}\text{I}$  [16] and was investigated in detail in the experiments of spontaneous fissions of  $^{248}\text{Cm}$  [4,5] and  $^{252}\text{Cf}$  [11]. The  $\gamma$  band ( $I^\pi = 3^+$ ,  $5^+$ , and  $7^+$  at 1305-, 1573-, and 1955-keV levels, respectively) in  $^{140}\text{Xe}$  was reported in the experiment of spontaneous fission of  $^{248}\text{Cm}$  [5]. However, Ref. [11] proposed the existence of  $s = \pm 1$  parity-doublet octupole bands and assignment of this positive-parity band as the  $s = -1$  octupole band. Reference [12] supported the interpretation of the  $\gamma$  band by additional

new data for  $^{140}\text{Xe}$  and by systematic study of the  $\gamma$  bands in  $N = 86$  isotopes of  $^{142}\text{Ba}$  and  $^{144}\text{Ce}$ .

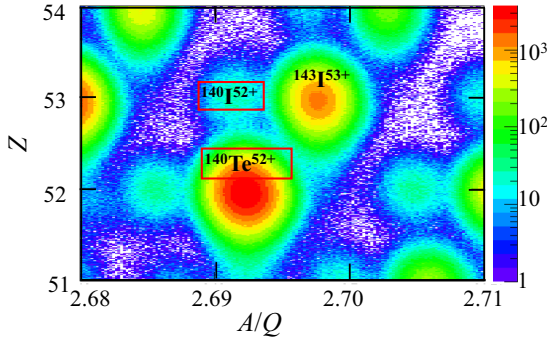
In this work, the experiment for the  $\beta$  decay of  $^{140}\text{I}$  to  $^{140}\text{Xe}$  was performed as one of experiments in the Euroball RIKEN Cluster Array (EURICA) project [18,19] at RIKEN. The aim of this project was to study nuclear structure in exotic nuclei far from the  $\beta$ -stability line based on  $\beta$ - and isomer-decay spectroscopy. The RI beam factory (RIBF) at the RIKEN Nishina Center can provide neutron-rich and neutron-deficient nuclei beyond previous detection limits on the nuclear chart by using in-flight fission of a U beam or projectile-fragmentation reaction of heavy-ion beams.

This paper is organized as follows. In Sec. II, experimental conditions are presented. In Sec. III, data analysis and the experimental results for the  $\beta$  decays of the ground state (g.s.) and new isomers in  $^{140}\text{I}$  to  $^{140}\text{Xe}$  are described in detail. In Sec. IV, nuclear structure of the g.s. and the isomers in  $^{140}\text{I}$ , and low-lying states in  $^{140}\text{Xe}$ , are discussed. Some levels are compared to theoretical calculations on a large-scale shell model and on the deformed Skyrme Hartree-Fock-Bogoliubov (HFB) plus deformed quasiparticle random-phase approximation (QRPA). In Sec. V, a summary of this work is presented.

## II. EXPERIMENT

Neutron-rich nuclei were produced by in-flight fission of a 345-MeV/nucleon  $^{238}\text{U}$  beam with an average intensity of 5 pnA, which bombarded a 3-mm-thick Be target, at RIBF, RIKEN. Neutron-rich Sb, Te, I, Xe, and Cs isotopes with  $A \sim 140$  were transported based on an in-flight separation technique by using the BigRIPS separator and ZeroDegree Spectrometer (ZDS) [20] up to the last focal plane (F11) with setting the magnetic rigidity ( $B\rho$ ) for  $^{142}\text{Te}^{52+}$  in this work. Particle identification (PI) of these isotopes was performed on the basis of time of flight (TOF),  $B\rho$ , and energy loss of the isotopes to deduce mass-to-charge ratio ( $A/Q$ ) and atomic number ( $Z$ ). Figure 1 shows plots of  $Z$  and  $A/Q$  for PI.

The isotopes were implanted into a position-sensitive active stopper, the Wide-range Active Silicon Strip Stopper Array for Beta and Ion detection (WAS3ABi) [18,19] installed at F11. This WAS3ABi consists of five double-sided Si strip detectors (DSSSDs) with 40 mm  $\times$  60 mm  $\times$  1 mm dimensions and with a segmentation of electrically 40 horizontal and 60 vertical strips in front and back sides, respectively. In addition, the WAS3ABi was used as a  $\beta$  counter for  $\beta$  decay of the fission fragments implanted inside it. Parent  $\beta$ -decaying nuclei were identified by position correlation of the implanted fragments with information of PI and the detected  $\beta$  rays in WAS3ABi. The isotopes with low rate of approximately 50 pps were implanted into WAS3ABi to reduce background components caused by the incorrect assignment between the implanted ions and the  $\beta$  rays.  $\gamma$  rays emitted after the  $\beta$

FIG. 1. Plots of  $Z$  vs  $A/Q$  for particle identification.

decay were detected by a  $\gamma$ -ray detector array, EURICA [18,19], surrounding the WAS3ABi. This EURICA consists of 12 cluster-type high-purity Ge detectors with seven crystals.

Relative intensity of the  $\gamma$  rays was obtained by using  $\gamma$ -ray photo-peak efficiency of the EURICA Ge array with distribution of the  $^{140}\text{Te}$  and  $^{140}\text{I}$  particles on five DSSSDs in WAS3ABi. This efficiency was simulated by GEANT4 [21], a toolkit for the Monte Carlo simulation for the passage of radiation through matter. Reliability of this simulation was confirmed by using the data of  $\gamma$ -ray standard point sources ( $^{133}\text{Ba}$  and  $^{152}\text{Eu}$ ) which were installed outside of the plastic scintillators upstream and downstream of WAS3ABi. Experimental  $\gamma$ -ray photo-peak efficiency obtained by using these two point sources is well reproduced by GEANT4 simulation. This method was described in detail in Ref. [22].

To study the  $\beta$  decay of  $^{140}\text{I}$  in this work, two data sets with PI of hydrogenlike  $^{140}\text{I}^{52+}$  and fully stripped  $^{140}\text{Te}^{52+}$  were analyzed. These particles can be seen in plots of  $Z$  vs  $A/Q$  for PI, as shown in Fig. 1. These data allow to study the  $\beta$  decays of (i)  $^{140}\text{I} \rightarrow ^{140}\text{Xe}$  and (ii)  $^{140}\text{Te} \rightarrow ^{140}\text{I} \rightarrow ^{140}\text{Xe}$ , respectively. Namely, the parent nucleus  $^{140}\text{I}$  was produced by two different reactions of (i) direct in-flight fission at a primary target and (ii)  $\beta$  decay of  $^{140}\text{Te}$  inside WAS3ABi. The numbers of implanted ions of  $^{140}\text{I}^{52+}$  and  $^{140}\text{Te}^{52+}$  in WAS3ABi are  $1.3 \times 10^4$  and  $3.1 \times 10^6$ , respectively, for around 3 days of measurement.

### III. DATA ANALYSIS AND EXPERIMENTAL RESULTS

#### A. Isomers in $^{140}\text{I}$

##### 1. High-spin isomer in $^{140}\text{I}$

$\gamma$ -ray energy spectra with PI of  $^{140}\text{I}$  and  $^{140}\text{Te}$  in Figs. 2(a) and 2(b), respectively, are coincident with  $\beta$  rays and set to a  $\beta$ - $\gamma$  time difference  $\{\Delta T(\beta\text{-}\gamma)\}$  of  $\pm 1.5 \mu\text{s}$ . Time windows between the particle and the  $\beta$  ray detected by WAS3ABi  $\{\Delta T(\text{particle-}\beta)\}$  are set to be 0–1.8 and 0.3–2.5 s in Figs. 2(a) and 2(b), respectively. These time windows enable to enhance the  $\gamma$  rays in  $^{140}\text{Xe}$  as daughter and grand-daughter nuclei from the  $\beta$  decays of the parent nuclei of  $^{140}\text{I}$  ( $^{140}\text{I} \rightarrow ^{140}\text{Xe}$ ) and  $^{140}\text{Te}$  ( $^{140}\text{Te} \rightarrow ^{140}\text{I} \rightarrow ^{140}\text{Xe}$ ) with half-lives of 0.553(46) s [23] and 0.350(5) s [24], respectively.

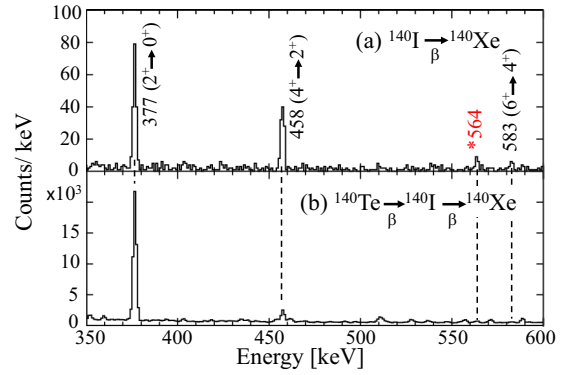


FIG. 2.  $\gamma$ -ray energy spectra in coincidence with  $\beta$  ray for the  $\beta$  decays of (a)  $^{140}\text{I} \rightarrow ^{140}\text{Xe}$  and (b)  $^{140}\text{Te} \rightarrow ^{140}\text{I} \rightarrow ^{140}\text{Xe}$  with  $\Delta T$  (particle- $\beta$ ) of 0–1.8 and 0.3–2.5 s, respectively.  $\gamma$  ray labeled with \* (indicated in red) is newly observed.

$\gamma$  rays of 377 and 458 keV are surprisingly observed with different intensity ratios  $\{I(458)/I(377)\}$  of 65(9)% and 11.4(8)% in the spectra of the  $\beta$  decays of  $^{140}\text{I} \rightarrow ^{140}\text{Xe}$  and  $^{140}\text{Te} \rightarrow ^{140}\text{I} \rightarrow ^{140}\text{Xe}$ , as shown in Figs. 2(a) and 2(b), respectively. These transitions were reported as the  $\gamma$  rays of 377 keV ( $2^+ \rightarrow 0^+$ ) and 458 keV ( $4^+ \rightarrow 2^+$ ) emitted after the  $\beta$  decay of  $^{140}\text{I}$  to  $^{140}\text{Xe}$  with  $\{I(458)/I(377)\}$  of 70(4)% in Ref. [16]. For the  $\beta$  decay of  $^{140}\text{Te} \rightarrow ^{140}\text{I} \rightarrow ^{140}\text{Xe}$ , levels of the daughter nucleus  $^{140}\text{I}$  are populated by the  $\beta$  decay of the g.s. ( $0^+$ ) in  $^{140}\text{Te}$ . This suggests that directly populated levels in  $^{140}\text{I}$  have spins and parities ( $I^\pi$ ) of  $1^+$  and  $0^- - 2^-$  by the selection rule of allowed and first-forbidden  $\beta$ -decay transitions, respectively. On the other hand, for the  $\beta$  decay of  $^{140}\text{I} \rightarrow ^{140}\text{Xe}$ , high-spin states in  $^{140}\text{I}$  can be populated, because the  $^{140}\text{I}$  particle is produced by in-flight fission. This indicates that the observed difference of  $\{I(458)/I(377)\}$  is caused by the  $\beta$  decays of the high-spin and low-spin states in  $^{140}\text{I}$ . Therefore, we propose a new  $\beta$ -decay isomer in  $^{140}\text{I}$ .

Location of this new isomer in the level scheme of  $^{140}\text{I}$  is investigated by the data analysis of the  $\beta$  decay of  $^{140}\text{Te} \rightarrow ^{140}\text{I} \rightarrow ^{140}\text{Xe}$  from the correlation between the  $\gamma$  ray ( $\gamma_1$ ) in the daughter nucleus  $^{140}\text{I}$  and the  $\gamma$  ray ( $\gamma_2$ ) in the grand-daughter nucleus  $^{140}\text{Xe}$ , as shown in Fig. 3(a). This analysis is possible by using the absolute time information of time stamps for the detection of particles and  $\beta$  rays in WAS3ABi. The  $\gamma_1$  is observed in  $\Delta T(\text{particle-}\beta_1)$  of 0–1 s, while the  $\gamma_2$  is observed in the time difference between the first and the second detected  $\beta$  rays  $\{\Delta T(\beta_1\text{-}\beta_2)\}$  of 0–1.5 s. Figure 3(b) shows a schematic of a two-dimensional  $\gamma$ - $\gamma$  matrix with  $\gamma$ -ray energy of  $E_{\gamma_1}$  for  $^{140}\text{Te} \rightarrow ^{140}\text{I}$  and  $E_{\gamma_2}$  for  $^{140}\text{I} \rightarrow ^{140}\text{Xe}$  in the  $\beta$  decay of  $^{140}\text{Te} \rightarrow ^{140}\text{I} \rightarrow ^{140}\text{Xe}$  data. Study of the  $^{140}\text{Xe}$   $\gamma$ -ray ( $\gamma_2$ ) energy spectra gated by the  $^{140}\text{I}$   $\gamma$  ray ( $\gamma_1$ ) enables to search for the  $\beta$ -decay isomeric state in  $^{140}\text{I}$ . Figure 3(c) shows the sum of  $^{140}\text{Xe}$   $\gamma$ -ray ( $\gamma_2$ ) energy spectra gated by the  $^{140}\text{I}$   $\gamma$  rays ( $\gamma_1$ ; 51, 121, 142, 186, and 342 keV) populating the g.s. in  $^{140}\text{I}$ .  $\gamma$  rays observed in Fig. 3(c) are suggested to be emitted after the  $\beta$  decay of the g.s. in  $^{140}\text{I}$ . The 377- and 458-keV  $\gamma$  rays can be seen in this figure with small  $I(458)/I(377)$  ratio. However, a large  $I(458)/I(377)$  ratio is observed in the  $^{140}\text{Xe}$   $\gamma$ -ray ( $\gamma_2$ ) energy spectrum gated on

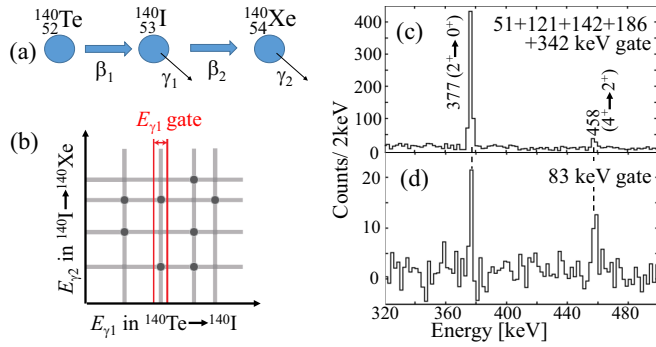


FIG. 3. (a) Chain of the  $\beta$  decay of  $^{140}\text{Te} \rightarrow ^{140}\text{I} \rightarrow ^{140}\text{Xe}$ . (b) Schematic two-dimensional  $\gamma$ - $\gamma$  matrix with energy of  $E_{\gamma_1}$  in  $^{140}\text{Te} \rightarrow ^{140}\text{I}$  ( $x$  axis) and  $E_{\gamma_2}$  in  $^{140}\text{I} \rightarrow ^{140}\text{Xe}$  ( $y$  axis) is displayed for the  $\beta$  decay of  $^{140}\text{Te} \rightarrow ^{140}\text{I} \rightarrow ^{140}\text{Xe}$ .  $\gamma$ -ray ( $\gamma_2$  in  $^{140}\text{Xe}$ ) energy ( $E_{\gamma_2}$ ) spectra are gated by the  $^{140}\text{I}$   $\gamma$  rays ( $\gamma_1$ ) (c) populating the g.s. and (d) correlating the isomer in  $^{140}\text{I}$ .

the new  $^{140}\text{I}$   $\gamma$  ray ( $\gamma_1$ ) of 83 keV, as shown in Fig. 3(d). This means that the 83-keV  $\gamma$  ray is correlated to the isomer in  $^{140}\text{I}$  and  $\gamma$  rays observed in Fig. 3(d) are suggested to be emitted after the  $\beta$  decay of the isomer in  $^{140}\text{I}$ . Due to the large  $I(458; 4^+ \rightarrow 2^+)/I(377; 2^+ \rightarrow \text{g.s.})$ , this isomer in  $^{140}\text{I}$  is proposed to have higher spin than that of the g.s.

The  $\beta$  decay of  $^{140}\text{Te}$  to  $^{140}\text{I}$  was studied by using the same EURICA data in Ref. [24] and a part of the reported decay scheme including new transitions and a level with \* (in red) are displayed in Fig. 4(a). The excitation energy ( $E_x$ ) of the level populated by the 83-keV  $\gamma$  ray in  $^{140}\text{I}$  is confirmed by the analysis of  $\gamma$ - $\gamma$  coincidence data for the  $\gamma$  rays in  $^{140}\text{I}$  emitted after the  $\beta$  decay of  $^{140}\text{Te}$  in  $\Delta T(^{140}\text{Te} \text{ particle-}\beta)$  of 0–1 s and in the time difference between two  $\gamma$  rays of  $|\Delta T(\gamma\text{-}\gamma)| < 300$  ns. Figure 4(b) shows the sum of  $\gamma$ -ray energy spectra gated by the reported 805- and 1067-keV  $\gamma$  rays which populate the 121-keV level in  $^{140}\text{I}$ . New  $\gamma$  rays of 83 and 70 keV as well as the reported  $\gamma$  rays of 78 and 121 keV depopulating the 121-keV level can be seen in Fig. 4(b). The 70-keV  $\gamma$  ray can be assigned as the transition between

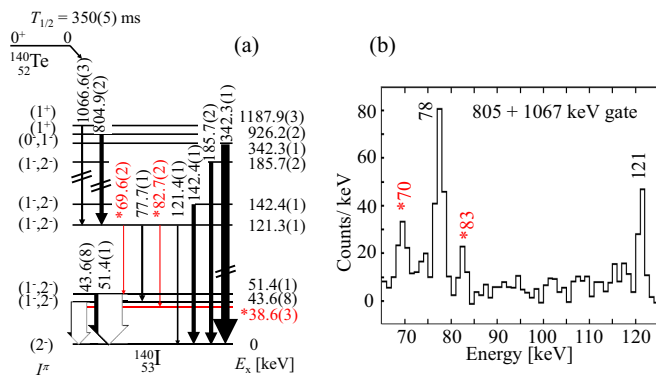


FIG. 4. (a) Partial  $\beta$ -decay scheme in  $^{140}\text{Te} \rightarrow ^{140}\text{I}$  (in black [24]) and (b) sum of  $^{140}\text{I}$   $\gamma$ -ray spectra gated by the 805- and 1067-keV transitions in  $^{140}\text{I}$ .  $\gamma$  rays and a level labeled with \* (in red) are newly found in this work.

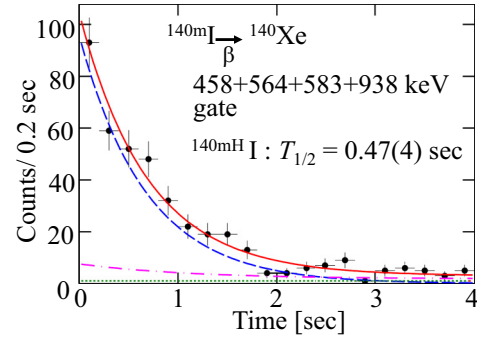


FIG. 5. Sum of time-difference (between  $^{140}\text{I}$  implantation and  $\beta$ -decay event) spectra gated by the  $\gamma$  rays of 458, 564, 583, and 938 keV in  $^{140}\text{Xe}$ . The decay curve (solid line, red) consists of the  $\beta$  decay of the HSI in  $^{140}\text{I}$  (dashed line, blue), Compton scattering (dot-dashed line, pink), and background (dotted line, green) components.

previously reported levels of 51 and 121 keV, because the energy difference of 69.9(1) keV [ $121.3(1) - 51.4(1)$  keV] is consistent with the  $\gamma$ -ray energy of 69.6(2) keV. The 83-keV transition is suggested to depopulate the 121-keV level and populate the new 38.6(3)-keV level. This level at 39 keV or another level at  $(39 - x)$  keV ( $x$  corresponding to very low energy) is supposed to originate the  $\beta$ -decay of the high-spin isomer (HSI) in  $^{140}\text{I}$ .

The half-life ( $T_{1/2}$ ) for the  $\beta$  decay of the HSI in  $^{140}\text{I}$  is determined with data analysis of the time difference between  $^{140}\text{I}$  implantation and the  $\beta$ -decay event at the same position in WAS3ABi. Additionally, the time-difference spectra are gated on the  $^{140}\text{Xe}$   $\gamma$  transitions populating the states with high spin ( $I > 3$ ), because the HSI in  $^{140}\text{I}$  are expected to strongly  $\beta$  decay to the high-spin states in  $^{140}\text{Xe}$ . Figure 5 shows the sum of time-difference spectra gating on the  $\gamma$  rays of 458 keV ( $4^+ \rightarrow 2^+$ ), 583 keV ( $6^+ \rightarrow 4^+$ ), and 938 keV ( $5^- \rightarrow 4^+$ ) as well as a newly observed  $\gamma$  ray of 564 keV ( $\rightarrow 4^+$ ), whose location in the decay scheme is described in Sec. III B 1. The decay curve (solid line, red) consists of the  $\beta$  decay of the HSI in  $^{140}\text{I}$  (dashed line, blue), Compton scattering (dot-dashed line, pink), and background (dotted line, green) components with fit by the maximum-likelihood method. As a result,  $T_{1/2}$  of the  $\beta$  decay of the HSI in  $^{140}\text{I}$  is determined to be 0.47(4) s.

## 2. Low-spin isomer in $^{140}\text{I}$

As spin of the g.s. in  $^{140}\text{I}$  is proposed to be lower than that of the HSI, data with  $^{140}\text{Te}$  PI are analyzed to determine the  $T_{1/2}$  for the  $\beta$  decay of the g.s. in  $^{140}\text{I}$ . By the  $\beta$  decay of  $^{140}\text{Te}$  ( $0^+$ ), low-spin states in  $^{140}\text{I}$  are expected to be populated based on the  $\beta$ -decay selection rule. Figure 6(a) shows the sum of spectra of the time difference between  $^{140}\text{Te}$  implantation and the  $\beta$ -decay event in WAS3ABi gated on the  $\gamma$  rays of 679 keV ( $3^- \rightarrow 4^+$ ) and 1136 keV ( $3^- \rightarrow 2^+$ ) after subtracting the Compton component. These  $\gamma$  rays were reported as the transitions emitted after the  $\beta$  decay of  $^{140}\text{I}$  to  $^{140}\text{Xe}$  [16]. This decay curve (solid line, red) fitted by the least-squares method consists of the time distributions of the  $\beta$ -decay component of  $^{140}\text{Te}$  ( $T_{1/2} = 0.350(5)$  s [24])  $\rightarrow ^{140}\text{I} \rightarrow ^{140}\text{Xe}$  (dashed line, blue) and background (dotted line, green). From this decay

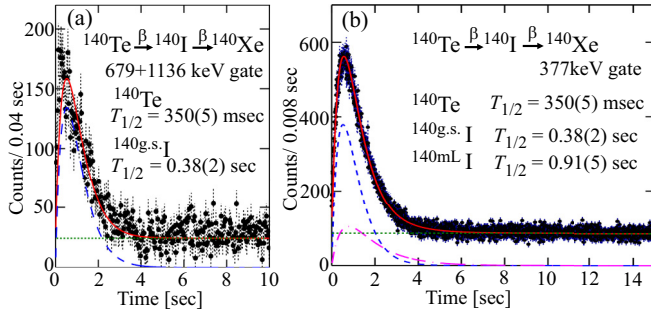


FIG. 6. (a) Sum of time-difference (between  $^{140}\text{Te}$  implantation and  $\beta$ -decay event) spectra gated by the 679- and 1136-keV  $\gamma$  rays in  $^{140}\text{Xe}$ . The decay curve (solid line, red) consists of sequential  $\beta$  decay of  $^{140}\text{Te} \rightarrow ^{140}\text{I}$  (g.s.)  $\rightarrow ^{140}\text{Xe}$  (dashed line, blue) and background (dotted line, green) components. (b) The time-difference spectrum gated by the 377-keV  $\gamma$  ray in  $^{140}\text{Xe}$  is displayed. The decay curve (solid line, red) consists of two sequential  $\beta$  decays of  $^{140}\text{Te} \rightarrow ^{140}\text{I}$  (g.s. and LSI)  $\rightarrow ^{140}\text{Xe}$  (dashed line, blue and dot-dashed line, pink, respectively) and background (dotted line, green) components.

curve,  $T_{1/2}$  for the  $\beta$  decay of the g.s. in  $^{140}\text{I}$  is determined to be 0.38(2) s. This  $T_{1/2}$  is shorter than 0.47(4) s for that of the HSI in  $^{140}\text{I}$  determined in this work. These  $T_{1/2}$  are not consistent with the reported value of 0.553(46) s deduced from the time distribution of  $\beta$  rays in the  $\beta$  ray of  $^{140}\text{I}$  from the same EURICA data [23]. And also, these  $T_{1/2}$  do not correspond to the reported values of 0.59(1) and 0.86(4) s, which were determined in experiments of fission fragments using a mass separation system [25] and a gas-flow system [26,27], respectively. To solve this discrepancy between these  $T_{1/2}$ , an additional isomer may be expected with longer  $T_{1/2}$  than those of the g.s. and the HSI in  $^{140}\text{I}$ . A time-difference spectrum gated by the most intense 377-keV ( $2^+ \rightarrow 0^+$ )  $\gamma$  ray in  $^{140}\text{Xe}$  is analyzed with two sequential  $\beta$  decays of  $^{140}\text{Te} \rightarrow ^{140}\text{I}$  (g.s. or second isomer)  $\rightarrow ^{140}\text{Xe}$ , as shown in Fig. 6(b). This decay curve (solid line, red) is fitted by the least-squares method. The  $\beta$ -decay component with longer half-life of 0.91(5) s (dashed line, pink) is additionally found with components of  $\beta$  decay of the g.s. in  $^{140}\text{I}$  with  $T_{1/2}$  of 0.38(2) s (dot-dashed line, blue) and background (dotted line, green). This suggests that another new isomer with  $T_{1/2}$  of 0.91(5) s is found in this work. And this isomer is supposed to have lower spin than those of the HSI and the g.s., because no  $\beta$ -decay component with  $T_{1/2}$  of 0.91 s is observed in the time-difference spectrum for the  $\beta$  decay of the g.s. in  $^{140}\text{I}$ , as shown in Fig. 6(a). This  $T_{1/2}$  of 0.91(5) s corresponds to 0.86(4) s [26,27]. Therefore, the half-lives of 0.553(46) s [23] and 0.59(1) s [25] are presumed to correspond to a mixture of the components of the  $\beta$  decay of the g.s., HSI, and this low-spin isomer (LSI) in  $^{140}\text{I}$ .

As a summary of this section, two  $\beta$ -decay isomers are newly found in  $^{140}\text{I}$ . The  $T_{1/2}$  of the  $\beta$  decays of the g.s., the LSI, and the HSI are determined to be 0.38(2), 0.91(5), and 0.47(4) s, respectively.

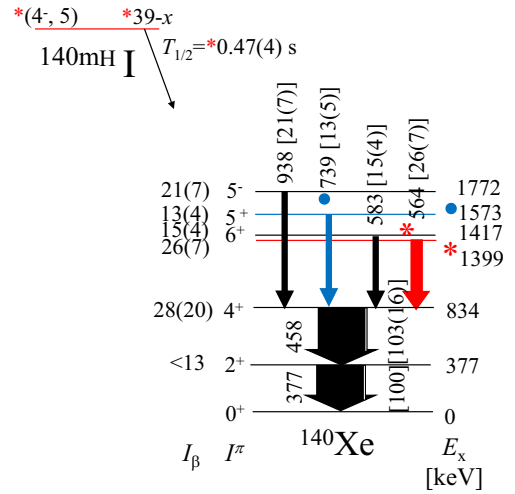


FIG. 7. Decay scheme of the  $\beta$  decay of the HSI in  $^{140}\text{I}$ . One  $\gamma$  transition and one level labeled with \* (in red) are newly found in this work. Those with • (in blue) reported in Refs. [5,11] are newly assigned to ones associated with the  $\beta$  decay of  $^{140}\text{I}$ . Spin and parity ( $I^\pi$ ) are taken from Ref. [27]. The intensity of the  $\gamma$  ray and  $\beta$  ray ( $I_\beta$ ) are normalized to the 377-keV  $\gamma$ -ray intensity.

## B. Construction of $\beta$ -decay scheme of $^{140}\text{I}$ to $^{140}\text{Xe}$

### 1. $\beta$ decay of high-spin isomer in $^{140}\text{I}$ to $^{140}\text{Xe}$

$\gamma$  rays of 377, 458, 564, 583, 739, and 938 keV in  $^{140}\text{Xe}$  are assigned as transitions emitted after the  $\beta$  decay of the HSI in  $^{140}\text{I}$  by analysis of data with  $^{140}\text{I}$  PI.  $\gamma$  rays of 377 keV ( $2^+ \rightarrow 0^+$ ), 458 keV ( $4^+ \rightarrow 2^+$ ), 583 keV ( $6^+ \rightarrow 4^+$ ), and 938 keV ( $5^- \rightarrow 4^+$ ) were reported in Ref. [16]. The 739-keV  $\gamma$  ray, which was reported as a transition ( $5^+$  at 1573 keV  $\rightarrow 4^+$  at 834 keV) in fission-fragment experiments [5,11], is newly assigned as a transition emitted after the  $\beta$  decay of  $^{140}\text{I}$ . The 564-keV  $\gamma$  ray is newly found as a transition in  $^{140}\text{Xe}$ . By  $\gamma$ - $\gamma$  coincidence analysis for the  $\gamma$  rays in  $^{140}\text{Xe}$  emitted after the  $\beta$  decay of  $^{140}\text{I}$  with  $^{140}\text{I}$  PI with  $\Delta T$  (particle- $\beta$ ) of 0–1.8 s, the 564-keV transition is found to be coincident with the 377- and 458-keV  $\gamma$  rays and not to be coincident with the 583-, 739-, and 938-keV  $\gamma$  rays. From this coincidence relation, the 564-keV transition is suggested to populate the  $4^+$  level at 834 keV and to depopulate the new level at 1399 keV.

By using this information, the decay scheme of the  $\beta$  decay of the HSI in  $^{140}\text{I}$  is proposed in Fig. 7. One transition and one level are newly found in this work.

### 2. $\beta$ decays of ground state and low-spin isomer in $^{140}\text{I}$ to $^{140}\text{Xe}$

Figure 8 shows the  $\gamma$ -ray energy spectrum gated by the 377-keV ( $2^+ \rightarrow 0^+$ ) transition in  $^{140}\text{Xe}$  by analysis of data with  $^{140}\text{Te}$  PI,  $\Delta T$  (particle- $\beta$ ) of 0.3–2.5 s, and  $|\Delta T(\gamma\text{-}\gamma)| < 300$  ns.  $\gamma$  rays observed in Fig. 8 including 46 new  $\gamma$  transitions are associated with the  $\beta$  decay of the g.s. and/or the LSI in  $^{140}\text{I}$ . The 458-keV ( $4^+ \rightarrow 2^+$ ), 679-keV ( $3^- \rightarrow 4^+$ ), and 1136-keV ( $3^- \rightarrow 2^+$ )  $\gamma$  rays were reported in the  $\beta$  decay of  $^{140}\text{I}$  to  $^{140}\text{Xe}$  [16], although the  $\gamma$ -ray intensities of these transitions are much smaller in this work. The 928-, 1194-, and 1588-keV  $\gamma$  rays, which were tentatively assigned in Fig. 1 of

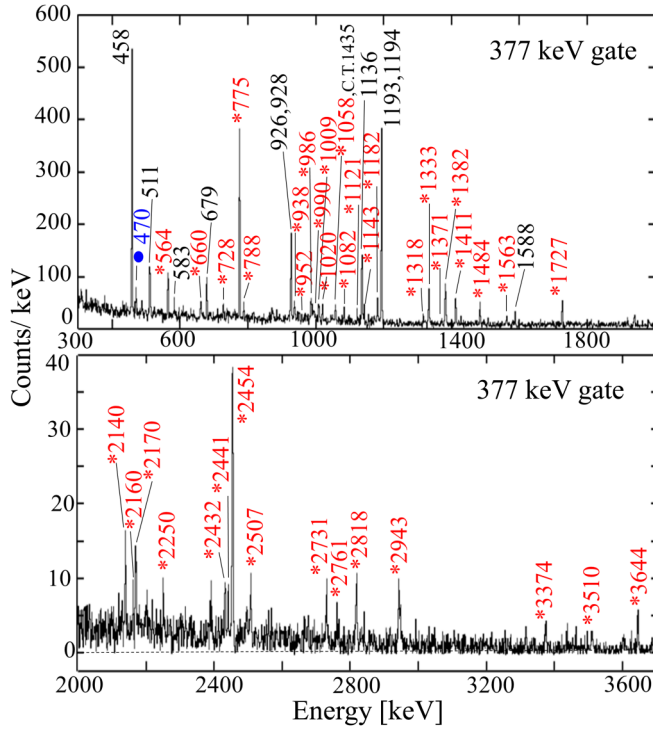


FIG. 8.  $\gamma$ -ray energy spectrum gated on the 377-keV transition in  $^{140}\text{Xe}$  by analysis of data with  $^{140}\text{Te}$  PI with  $\Delta T$  (particle- $\beta$ ) of 0.3–2.5 s, and  $|\Delta T(\gamma-\gamma)| < 300$  ns.  $\gamma$  rays in  $^{140}\text{Xe}$  labeled with \* (in red) are newly found in this work. That with • (in blue) reported in Refs. [5,11] is newly assigned as a transition emitted after the  $\beta$  decay of  $^{140}\text{I}$ . C.T. stands for crosstalk.

Ref. [16], are observed in the present work. In this reference, a tentatively assigned transition of 1765 keV ( $\rightarrow 2^+$ ), those of 998, 1049, 1765, 2377, and 2413 keV ( $\rightarrow 4^+$ ), and that of 258 keV ( $5^- \rightarrow 3^-$ ) are not observed in this work. The 470-keV ( $3^+ \rightarrow 4^+$ ) transition is newly assigned to a transition emitted after the  $\beta$  decay of  $^{140}\text{I}$  to  $^{140}\text{Xe}$ , although this was reported in experiments of spontaneous-fission fragments of  $^{248}\text{Cm}$  [5] and  $^{252}\text{Cf}$  [11].

$\gamma$  transitions directly populating the g.s. in  $^{140}\text{Xe}$  were investigated comparing the  $\gamma$ -ray energy spectrum coincident

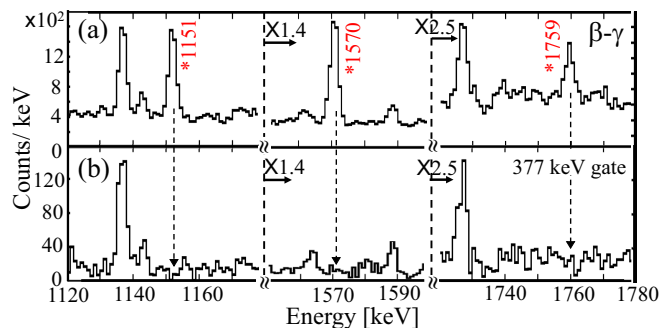


FIG. 9.  $\gamma$ -ray energy spectra (a) coincident with  $\beta$  ray and (b) gated by the 377-keV  $\gamma$  ray in  $^{140}\text{Xe}$  under the same conditions as Figs. 2(b) and 8, respectively.  $\gamma$  rays labeled with \* (in red) are newly found in this work.

TABLE I. Coincidence relations of the  $\gamma$  rays in  $^{140}\text{Xe}$  from the analysis of data with  $^{140}\text{Te}$  PI.

Gate $\gamma$ ray (keV)	Coincident $\gamma$ ray (keV)	Gate $\gamma$ ray (keV)	Coincident $\gamma$ ray (keV)
458	377, 470, 564, 679, 926, 1009, (1020), 1058, 1193, (1318), 2507	1194	377, 952, 986, 994, 1484, 2140
470	377, 458, 660, (990), 1020	1318	377, 458, (679), 1136
564	377, 458, 926, 1058	1333	377
660	377, (458), 470, 928	1371	377, 775, 1151
679	377, 458, (1009), (1193), 1318, 2507	1382	377
728	377, (470), 775, 928, 990, 1143, 1151	1484	377, 1194, 1570
775	377, 728, 788, 1082, 1143, 1173, 1371, 1871	1570	(952), 986, 994, 1484, 2140
788	377, 775, 1151	1588	377
926	377, 458, 564	1727	377
928	377, 660, 728, 990, 1020	1759	None
952	377, 1194, 1570	1871	377, 775, 1151
986	377, 1194, 1570	2140	377, 1194, 1570
990	377, (470), 728, 928	2160	377
994	377, 1194, 1570	2170	377
1009	377, 458, (679), 1136	2250	377
1020	377, 458, 470, 928	2432	377
1058	377, 458, 564	2441	377
1082	377, 775, 1151	2454	377
1121	377	2507	377, 458, 679, 1136
1136	377, 1009, 1193, 1318, 2507	2731	377
1143	377, 728, 775, 1151	2761	377
1151	728, 788, 1082, 1143, 1173, 1371, 1871	2818	377
1173	377, 775, 1151	2943	377
1182	377	3374	377
1193	377, (458), (679), 1136	3510	377
		3644	377

with the  $\beta$  ray to that gated by the 377-keV  $\gamma$  ray ( $2^+ \rightarrow 0^+$ ), as shown in Figs. 9(a) and 9(b), respectively. As the 1151-, 1570-, and 1759-keV peaks are clearly observed in Fig. 9(a) and not in Fig. 9(b), these  $\gamma$  transitions are assigned to those directly populating the g.s. in  $^{140}\text{Xe}$ .

The 377-keV ( $2^+ \rightarrow 0^+$ ) transition was found to be coincident with 50  $\gamma$  transitions. Coincidence relations of all observed transitions in  $^{140}\text{Xe}$  are listed in Table I. By using these coincidence relations, the decay scheme of the mixed  $\beta$  decays of the g.s. and the LSI in  $^{140}\text{I}$  is constructed, as shown in Fig. 10. We note that two components of the  $\beta$  decays are not separated. As the  $E_x$  of the LSI cannot be determined,  $E(\text{LSI}) = y$  is written in Fig. 10. In this work, 35 excited levels are newly found. One level reported in references of the spontaneous fissions of  $^{248}\text{Cm}$  [3–5] and  $^{252}\text{Cf}$  [6–12] is newly assigned to the level populated by the  $\beta$  decay of the g.s. and/or the LSI in  $^{140}\text{I}$  to  $^{140}\text{Xe}$ . The detailed results

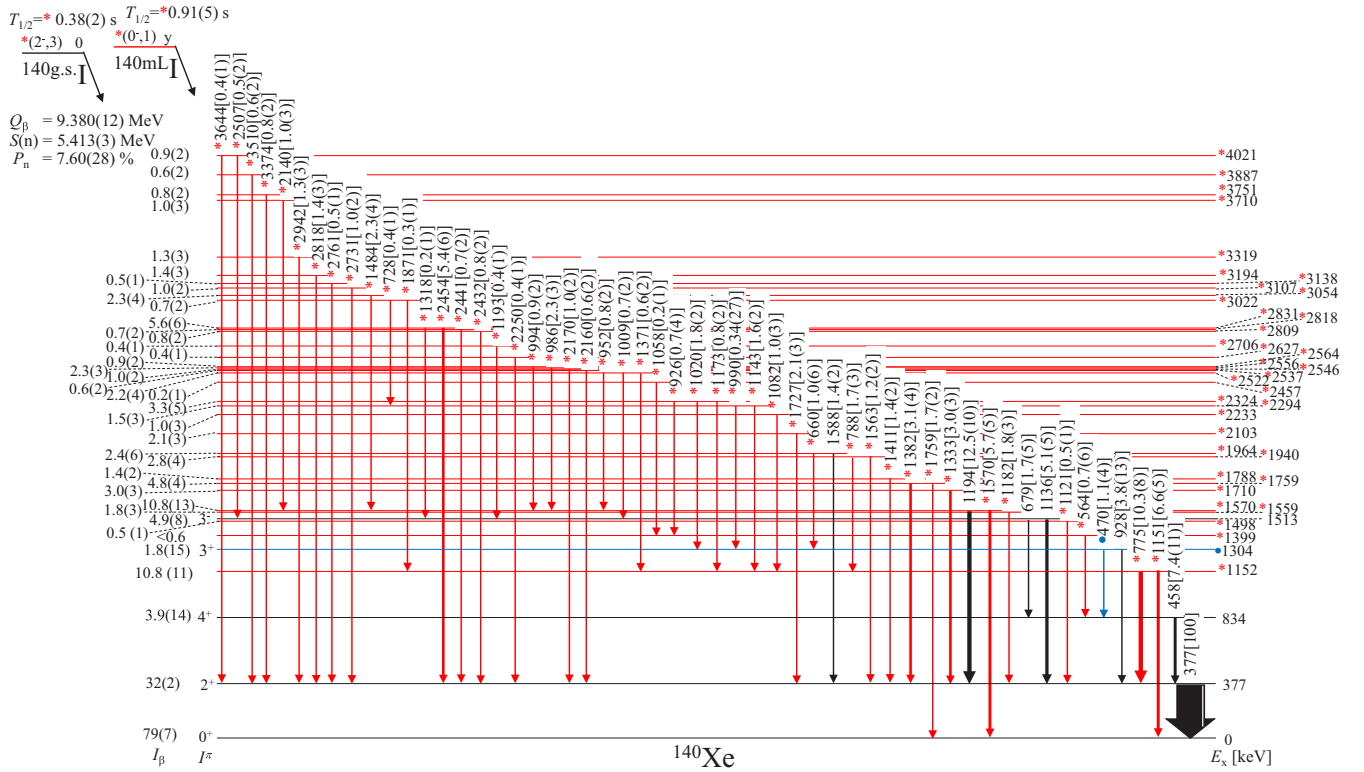


FIG. 10. Decay scheme of the mixed  $\beta$  decays of the g.s. and the LSI in  $^{140}\text{I}$ .  $\gamma$  transitions and levels labeled with \* (in red) are newly found in this work. Those with • (in blue) reported in Refs. [5,11] are newly assigned to ones associated with the  $\beta$  decay of  $^{140}\text{I}$ . Spin and parity ( $I^\pi$ ) are taken from Ref. [27]. The  $Q$  value of  $\beta$  decay ( $Q_\beta$ ), neutron separation energy ( $S_n$ ), and branching ratio of  $\beta$ -delayed neutron decay are taken from Refs. [28,29]. The intensities of  $\gamma$  ray and  $\beta$  ray ( $I_\beta$ ) are normalized to the 377-keV  $\gamma$ -ray intensity.

concerning the  $\gamma$  transitions and the excited states in  $^{140}\text{Xe}$  are listed in Table II.

### 3. Intensities of $\gamma$ and $\beta$ transitions

Intensities of  $\gamma$  rays in  $^{140}\text{Xe}$  emitted after the  $\beta$  decays of the g.s. + LSI and the HSI in  $^{140}\text{I}$  are listed in Table II. These intensities are obtained by using photo-peak efficiency including position distribution of the implanted particles in WAS3ABi based on the result of the GEANT4 simulation, which is described in Sec. II. The intensities of all  $\gamma$  transitions are normalized to that of the 377-keV ( $2^+ \rightarrow 0^+$ )  $\gamma$  ray. This 377-keV transition intensity is corrected by the internal-conversion intensity calculated by using the internal-conversion coefficient [27].

$\beta$ -decay intensity to each excited state in  $^{140}\text{Xe}$  is deduced by comparing the intensities of  $\gamma$  rays populating and depopulating each excited state. These  $\beta$ -decay intensities are also normalized to that of the 377-keV  $\gamma$  ray.  $\beta$  decay to the g.s. in  $^{140}\text{Xe}$  has to be considered in the case of the  $\beta$  decays of the g.s. + LSI in  $^{140}\text{I}$ . This value is obtained by comparing the total number of  $^{140}\text{Xe}$  particles to the sum of the intensities of  $\gamma$  rays populating the g.s. in  $^{140}\text{Xe}$ . The total number of  $^{140}\text{Xe}$  particles is estimated from the  $\gamma$ -ray intensity in  $^{140}\text{Cs}$ , which was reported in the study of the  $\beta$  decay of  $^{140}\text{Xe}$  to  $^{140}\text{Cs}$  [30]. As result, the relative intensity (normalized to the 377-keV  $\gamma$ -ray intensity) is obtained to be 79(7)% for the direct  $\beta$  decay of the g.s. + LSI in  $^{140}\text{I}$  to the g.s. in  $^{140}\text{Xe}$

by the analysis of the data with  $^{140}\text{Te}$  PI. No  $\beta$  decay of the HSI in  $^{140}\text{I}$  to the g.s. in  $^{140}\text{Xe}$  is suggested based on the first-forbidden  $\beta$  decay, because the  $6^+$  level in  $^{140}\text{Xe}$  is populated in this  $\beta$  decay. The excitation energies of each level in  $^{140}\text{Xe}$  and  $\beta$ -decay intensity to each level are summarized in Table III.

The HSI in  $^{140}\text{I}$  is supposed to be directly produced at the primary-target position by in-flight fission. The isomer ratio can be obtained comparing the numbers of particles with the HSI and the g.s. in  $^{140}\text{I}$  by analysis of data with  $^{140}\text{I}$  PI. The number of the HSI in  $^{140}\text{I}$  is deduced by using the  $\beta$ -decay component of the HSI of 60% in the absolute  $I_\gamma(377 \text{ keV})$  obtained from analysis of time-difference spectrum (between  $^{140}\text{I}$  implantation and  $\beta$ -decay event) gated by the 377-keV  $\gamma$  ray. The number of the g.s. in  $^{140}\text{I}$  is extracted by using the  $I_\gamma$  in the grand-daughter nucleus  $^{140}\text{Cs}$ . Comparing these numbers of the HSI and the g.s., the isomer ratio for the  $^{140}\text{I}$  RI beam is extracted to be 27(13)% in WAS3ABi.

## IV. DISCUSSION

### A. Ground and isomeric states in $^{140}\text{I}$

Isomers were reported in odd-odd  $^{136}\text{I}$  ( $N = 83$ ) [31] and  $^{138}\text{I}$  ( $N = 85$ ) isotopes [32], as shown in Fig. 11. In the nucleus  $^{136}\text{I}$ , the spin and parity ( $I^\pi$ ) of the  $\beta$ -decay isomer ( $T_{1/2} = 46.6 \text{ s}$ ) at 201 keV were proposed to be ( $6^-$ ).  $I^\pi$  of the g.s. and the first excited state at 87 keV were reported to

TABLE II. Observed  $\gamma$  rays in  $^{140}\text{Xe}$  emitted after the  $\beta$  decays of the g.s. + LSI and the HSI in  $^{140}\text{I}$ . Energy of  $\gamma$  ray ( $E_\gamma$ ), and excitation energy and spin-parity of initial ( $E_i, I_i^\pi$ ) and final ( $E_f, I_f^\pi$ ) states are listed.  $\gamma$ -ray intensity ( $I_\gamma$ ) is normalized to that of the 377-keV transition intensity. This 377-keV  $\gamma$ -ray intensity is corrected by internal-conversion intensity. Spin and parity ( $I^\pi$ ) are taken from Ref. [27].

$E_\gamma$ (keV)	$E_i$ (keV)	$E_f$ (keV)	$I_i^\pi$ Ref. [27]	$I_f^\pi$	$I_\gamma$ (%)		$E_\gamma$ (keV)	$E_i$ (keV)	$E_f$ (keV)	$I_i^\pi$ Ref. [27]	$I_f^\pi$	$I_\gamma$ (%)	
					g.s.+LSI	HSI						g.s.+LSI	HSI
376.7(1)	377	0	2 <sup>+</sup>	0 <sup>+</sup>	100	100	1193.7(1)	1570	377		2 <sup>+</sup>	12.5(10)	
457.7(1)	834	377	4 <sup>+</sup>	2 <sup>+</sup>	7.4(11)	103(16)	1317.5(2)	2831	1513		3 <sup>-</sup>	0.2(1)	
469.7(1)	1304	834	3 <sup>+</sup>	4 <sup>+</sup>	1.1(4)		1332.8(1)	1710	377		2 <sup>+</sup>	3.0(3)	
564.2(1)	1399	834		4 <sup>+</sup>	0.7(6)	26(7)	1370.6(2)	2522	1152			0.6(2)	
582.5(2)	1417	834	6 <sup>+</sup>	4 <sup>+</sup>		15(4)	1382.2(2)	1759	377		2 <sup>+</sup>	3.1(4)	
659.8(2)	1964	1304		3 <sup>+</sup>	1.0(6)		1411.4(2)	1788	377		2 <sup>+</sup>	1.4(2)	
678.9(1)	1513	834	3 <sup>-</sup>	4 <sup>+</sup>	1.7(5)		1483.8(2)	3054	1570			2.3(4)	
728.0(3)	3022	2294			0.4(1)		1562.9(3)	1940	377		2 <sup>+</sup>	1.2(2)	
738.7(3)	1573	834	5 <sup>+</sup>	4 <sup>+</sup>		13(5)	1570.4(1)	1570	0		0 <sup>+</sup>	5.7(5)	
774.9(1)	1152	377		2 <sup>+</sup>	10.3(8)		1587.7(2)	1964	377		2 <sup>+</sup>	1.4(2)	
787.8(1)	1940	1152			1.7(3)		1726.6(2)	2103	377		2 <sup>+</sup>	2.1(3)	
926.0(2)	2324	1399			0.7(4)		1759.3(3)	1759	0		0 <sup>+</sup>	1.7(2)	
927.6(1)	1304	377	3 <sup>+</sup>	2 <sup>+</sup>	3.8(13)		1870.9(2)	3022	1152			0.3(1)	
937.5(1)	1772	834	5 <sup>-</sup>	4 <sup>+</sup>		21(7)	2139.9(2)	3710	1570			1.0(3)	
951.7(2)	2522	1570			0.8(2)		2160.1(3)	2537	377		2 <sup>+</sup>	0.6(2)	
985.9(2)	2556	1570			2.3(3)		2169.6(2)	2546	377		2 <sup>+</sup>	1.0(2)	
990.0(2)	2294	1304		3 <sup>+</sup>	0.34(27)		2250.3(2)	2627	377		2 <sup>+</sup>	0.4(1)	
993.7(2)	2564	1570			0.9(2)		2432.0(2)	2809	377		2 <sup>+</sup>	0.8(2)	
1009.0(1)	2522	1513		3 <sup>-</sup>	0.7(2)		2441.1(3)	2818	377		2 <sup>+</sup>	0.7(2)	
1020.2(2)	2324	1304		3 <sup>+</sup>	1.8(2)		2453.6(1)	2831	377		2 <sup>+</sup>	5.4(6)	
1058.0(2)	2457	1399			0.21(8)		2507.2(2)	4021	1513		3 <sup>-</sup>	0.5(2)	
1081.7(2)	2233	1152			1.0(3)		2730.5(2)	3107	377		2 <sup>+</sup>	1.0(2)	
1121.4(2)	1498	377		2 <sup>+</sup>	0.5(1)		2761.2(2)	3138	377		2 <sup>+</sup>	0.5(1)	
1136.4(1)	1513	377	3 <sup>-</sup>	2 <sup>+</sup>	5.1(5)		2817.5(1)	3194	377		2 <sup>+</sup>	1.4(3)	
1142.6(2)	2294	1152			1.6(2)		2942.5(1)	3319	377		2 <sup>+</sup>	1.3(3)	
1151.4(3)	1152	0		0 <sup>+</sup>	6.6(5)		3374.3(2)	3751	377		2 <sup>+</sup>	0.8(2)	
1172.7(2)	2324	1152			0.8(2)		3510.3(6)	3887	377		2 <sup>+</sup>	0.6(2)	
1181.8(1)	1559	377		2 <sup>+</sup>	1.8(3)		3644.0(2)	4021	377		2 <sup>+</sup>	0.4(1)	
1192.9(3)	2706	1513		3 <sup>-</sup>	0.4(1)								

TABLE III. Excitation energy ( $E_x$ ), spin and parity ( $I^\pi$ ), and  $\beta$ -ray intensity ( $I_\beta$ ) for the levels in  $^{140}\text{Xe}$  associated with the  $\beta$  decays of the g.s. + LSI and the HSI in  $^{140}\text{I}$ .  $I_\beta$  is normalized to the 377-keV  $\gamma$ -ray intensity. Spin and parity ( $I^\pi$ ) are taken from Ref. [27].

$E_x$ (keV)	$I^\pi$ Ref. [27]	$I_\beta$ (%)		$E_x$ (keV)	$I^\pi$ Ref. [27]	$I_\beta$ (%)		$E_x$ (keV)	$I^\pi$ Ref. [27]	$I_\beta$ (%)	
		g.s.+LSI	HSI			g.s.+LSI	HSI			g.s.+LSI	HSI
0	0 <sup>+</sup>	79(7)		1788.1(2)		1.4(2)		2808.7(3)		0.8(2)	
376.7(1)	2 <sup>+</sup>	32(2)	< 13	1939.5(2)		2.8(4)		2817.8(3)		0.7(2)	
834.4(1)	4 <sup>+</sup>	3.9(14)	28(20)	1964.3(2)		2.4(6)		2830.5(1)		5.6(6)	
1151.5(1)		10.8(11)		2103.3(2)		2.1(3)		3022.4(2)		0.7(2)	
1304.2(1)	3 <sup>+</sup>	1.8(15)		2233.3(2)		1.0(3)		3054.2(2)		2.3(4)	
1398.6(2)		<0.6	26(7)	2294.2(2)		1.5(3)		3107.2(2)		1.0(2)	
1416.9(2)	6 <sup>+</sup>		15(4)	2324.4(1)		3.3(5)		3137.9(3)		0.5(1)	
1498.1(2)		0.5(1)		2456.6(3)		0.2(1)		3194.2(1)		1.4(3)	
1513.2(1)	3 <sup>-</sup>	4.9(8)		2522.1(1)		2.2(4)		3319.2(2)		1.3(3)	
1558.5(2)		1.8(3)		2536.8(3)		0.6(2)		3710.2(3)		1.0(3)	
1570.4(1)		10.8(13)		2546.3(2)		1.0(2)		3751.0(3)		0.8(2)	
1573.1(3)	5 <sup>+</sup>		13(4)	2556.3(2)		2.3(3)		3887.0(6)		0.6(2)	
1709.5(1)		3.0(3)		2564.1(2)		0.9(2)		4020.6(2)		0.9(2)	
1759.1(1)		4.8(4)		2627.0(2)		0.4(1)					
1771.9(2)	5 <sup>-</sup>		21(7)	2706.1(3)		0.4(1)					

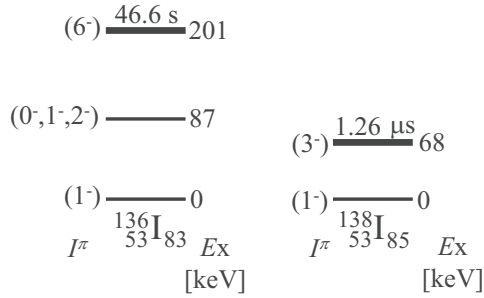


FIG. 11. Reported low-lying states including isomers (indicated by thick lines) in odd-odd  $^{136}\text{I}$  [31] and  $^{138}\text{I}$  [32] nuclei.

be  $(1^-)$  and  $(0^-, 1^-, 2^-)$ , respectively. This isomer is supposed to be a typical spin-gap isomer, which often appears in neighboring nuclei of a doubly-magic nucleus due to residual interaction between valence protons and valence neutrons. In the nucleus  $^{138}\text{I}$ ,  $I^\pi$  of the 1.26- $\mu\text{s}$  isomer at 68 keV was reported to be  $(3^-)$ . This isomer was explained to be caused by directly depopulating the low-energy  $E2$  transition. The excitation energy ( $E_x$ ) of the excited states in  $^{136}\text{I}$  and  $^{138}\text{I}$  were reproduced by the lowering of the  $\pi d_{5/2}$  orbital by  $-400$  and  $-600$  keV, respectively, in shell-model calculations [31,32]. This is supposed to induce larger configuration mixing with increase of neutron number. In this work for the nucleus  $^{140}\text{I}$  ( $N = 87$ ), two  $\beta$ -decay isomers are found. These isomers and the g.s. in  $^{140}\text{I}$  are discussed as follows.

The HSI in  $^{140}\text{I}$  is found to  $\beta$  decay to the levels at  $4^+$  ( $E_x = 834$  keV),  $6^+$  (1417),  $5^+$  (1573), and  $5^-$  (1772) in  $^{140}\text{Xe}$  with relative  $\beta$ -decay intensity of 28(20), 15(4), 13(4), and 21(7), respectively, normalized to the 377-keV  $\gamma$ -ray intensity, as shown in Fig. 7 and Table III. As both negative- and positive-parity levels in  $^{140}\text{Xe}$  are populated, these  $\beta$  decays of the HSI in  $^{140}\text{I}$  are suggested to be Gamow-Teller and first-forbidden transitions. If parity of the HSI is positive, this spin is expected to be 5. If it is negative, this spin is expected to be 4, 5, or 6. Assignment of  $6^-$  may be excluded because of no observation of  $\gamma$  rays depopulating the  $7^-$  level in  $^{140}\text{Xe}$ . As result, the probable candidate of the  $I^\pi$  of the HSI is supposed to be  $4^-, 5^-,$  and  $5^+$ .

The  $\beta$  decay of the g.s. in  $^{140}\text{I}$  is found (i) to be the main component in the sum of time-difference spectra gated by the 679-keV ( $3^- \rightarrow 4^+$ ) and by the 1136-keV ( $3^- \rightarrow 2^+$ ) transitions, as shown in Fig. 6(a), (ii) to be the component of 69% in the time-difference spectrum gated by the 377-keV ( $2^+ \rightarrow$  g.s.) transition, as shown in Fig. 6(b), and (iii) to populate weakly the  $4^+$  level. These indicate that spin of the g.s. is suggested to be 3 (if positive parity) and 2, 3, or 4 (if negative). Assignment of  $4^-$  may be excluded because of no observation of  $\gamma$  rays depopulating the  $5^-$  level. As result, the probable candidate of the  $I^\pi$  of the g.s. is supposed to be  $2^-, 3^-,$  and  $3^+$ .

The  $\beta$ -decay component of the LSI in  $^{140}\text{I}$  is found to be 33% in the time-difference spectrum gated by the 377-keV ( $2^+ \rightarrow$  g.s.) transition, as shown in Fig. 6(b). And this  $\beta$  decay populates the g.s. in  $^{140}\text{Xe}$  with large  $\beta$ -decay intensity of 79(7), as shown in Table III. These indicate that spin of

the LSI is supposed to be 1 (if positive parity) and 0, 1, or 2 (if negative). Assignment of  $2^-$  may be excluded because of no decay component with  $T_{1/2}$  of 0.91(5) s in the sum of time-difference spectra gated on the  $\gamma$  rays of 679 keV ( $3^- \rightarrow 4^+$ ) and 1136 keV ( $3^- \rightarrow 2^+$ ), as shown in Fig. 6(a). As a result, the probable candidate of the  $I^\pi$  of the LSI is supposed to be  $0^-, 1^-,$  and  $1^+$ .

Configuration of the g.s. and the low-lying states in the odd-odd nucleus  $^{140}\text{I}$  with 53 protons and 87 neutrons could be estimated from quasiparticle levels occupied by one quasiproton and one quasineutron coupled to an even-even nucleus  $^{138}\text{Te}$  ( $Z = 52$  and  $N = 86$ ). Each quasiproton and quasineutron could be deduced from the  $I^\pi$  of the g.s. in odd- $Z$  and odd- $N$  nuclei, respectively. For  $N = 87$  odd isotones,  $^{139}\text{Te}$  ( $Z = 52$ ) and  $^{141}\text{Xe}$  ( $Z = 54$ ),  $I^\pi$  of the g.s. was experimentally reported to be  $(7/2^-)$  [33] and  $5/2^{(-)}$  [34], respectively. This is assumed to indicate the quasineutron configurations of  $\nu 2f_{7/2}$  with spherical nature and of  $\nu[523]5/2^-$  with weak-quadrupole deformation for  $Z = 52$  and 54, respectively. Therefore, the nucleus  $^{140}\text{I}$  with  $Z = 53$  and  $N = 87$  could be located in the shape-transitional region from spherical to weak-quadrupole deformation. Next, for  $Z = 53$  odd isotopes,  $I^\pi$  of the g.s. in  $^{139}\text{I}$  ( $N = 86$ ) was experimentally reported to be  $(7/2^+)$  [33]. This suggests the quasiproton configuration of  $\pi 1g_{7/2}$  with spherical nature.  $I^\pi$  of the g.s. in  $^{141}\text{I}$  ( $N = 88$ ) has not yet been reported. However, the quasiproton configurations could be assumed to be  $\pi 1g_{7/2}$  with spherical nature and to be  $\pi[422]3/2^+$  with weak-quadrupole deformation. By using this information of the single-particle orbitals occupied by the 53rd quasiproton and the 87th quasineutron, a possible candidate of the  $I^\pi$  of the g.s. and low-lying states in  $^{140}\text{I}$  is supposed to be  $0^- - 7^-$  for  $\nu 2f_{7/2} \otimes \pi 1g_{7/2}$  with spherical nature and  $1^-, 4^-$  for  $\nu[523]5/2^- \otimes \pi[422]3/2^+$  with weak-prolate deformation as the lowest possible candidates.

From the  $\beta$ -decay selection rule,  $I^\pi$  of the g.s., the LSI, and the HSI are experimentally extracted to be  $(2^-, 3^-, 3^+)$ ,  $(0^-, 1^-, 1^+)$ , and  $(4^-, 5^-, 5^+)$ , respectively. Additionally, considering the estimation of  $I^\pi$  with combination between the 53rd quasiproton and the 87th quasineutron, candidates for  $I^\pi$  for the g.s., the LSI, and the HSI could be  $(2^-, 3^-)$ ,  $(0^-, 1^-)$ , and  $(4^-, 5^-)$ , respectively, with spherical shape. In case of weak-prolate deformation, candidates for  $I^\pi$  are proposed to be  $(1^-)$  and  $(4^-)$  for the LSI and the HSI, respectively.

These  $I^\pi$  of the g.s. and two isomers are also discussed comparing to a large-scale shell-model calculation whose framework was described in Refs. [35–38]. This shell-model calculation is carried out for  $^{140}\text{I}$  and  $^{140}\text{Xe}$  nuclei in this work. Single-particle levels in one-major shells, namely, six neutrons ( $2f_{7/2}$ ,  $3p_{3/2}$ ,  $3p_{1/2}$ ,  $1h_{9/2}$ ,  $2f_{5/2}$ , and  $1i_{13/2}$  orbitals) and five protons ( $1g_{7/2}$ ,  $2d_{5/2}$ ,  $2d_{3/2}$ ,  $1h_{11/2}$ , and  $3s_{1/2}$  orbitals) are considered. These single-particle energies are extracted from the excitation energies of low-lying states in  $^{133}\text{Sb}_{82}$  and  $^{133}\text{Sn}_{83}$ . A multipole-pairing plus quadrupole-quadrupole interaction is employed as an effective interaction. Interaction between neutrons and protons consists of only the quadrupole-quadrupole interaction. The fixed strengths are used to calculate for the neighboring nuclei around  $^{140}\text{I}$ . Results of this shell-model calculation for the low-lying states

with negative parity and spin of 0–6 are shown in Fig. 12. The theoretical  $E_x$  of the  $7^-$  level with 0.45 MeV is not plotted in this figure, because it is out of range. As theoretical  $E_x$  of the positive-parity states are higher than 2 MeV, these states are also not shown in the figure. The shell-model calculation predicts that the  $1^-$ ,  $2^-$ , and  $4^-$  levels appear as the three lowest-lying states. However, ordering of these states in energy could not be clearly reproduced because of theoretical errors of around 100 keV due to uncertainty of the interaction between proton and neutron. Comparing the experimental candidates for  $I^\pi$  of  $(2^-, 3^-, 3^+)$ ,  $(0^-, 1^-, 1^+)$ , and  $(4^-, 5^-, 5^+)$  for the g.s., the LSI, and the HSI in  $^{140}\text{I}$ , respectively, to theoretical calculation, the  $I^\pi$  is supposed to be  $(2^-)$ ,  $(1^-)$ , and  $(4^-)$ , respectively.

The  $I^\pi$  assignment of  $(4^-)$  for the HSI enables it to be a  $\beta$ -decay isomer with  $T_{1/2}$  of 0.47 s due to small transition probabilities of  $E2(4^-; \text{HSI} \rightarrow 2^-; \text{g.s.})$ , if  $E(\text{HSI})$  is very low, and of  $M3(4^-; \text{HSI} \rightarrow 1^-; \text{LSI})$ . However, the  $I^\pi$  assignment of  $(1^-)$  for the LSI does not allow a  $\beta$ -decay isomer with  $T_{1/2}$  of 0.91 s, because the transition probability of  $M1(1^-; \text{LSI} \rightarrow 2^-; \text{g.s.})$  is not so small even if  $E(\text{LSI})$  is very low. In the case of weak-prolate deformation, the estimated  $I^\pi$  are  $(1^-)$  and  $(4^-)$  for the LSI and the HSI, respectively, from the combination of the quasiproton and quasineutron. If the LSI has weak-prolate shape and the g.s. has spherical shape, the transition probability of  $M1(1^-; \text{LSI} \rightarrow 2^-; \text{g.s.})$  could be small because of different nuclear structure between the g.s. and the LSI. As the transition probability of  $M3(4^-; \text{HSI} \rightarrow 1^-; \text{LSI})$  is also small even if the HSI has spherical shape or weak-prolate shape, the LSI could become the  $\beta$ -decay isomer.

From the experimental, systematical, and theoretical suggestion,  $I^\pi$  of the g.s. may be presumed to be  $(2^-)$  with spherical shape,  $I^\pi$  of the LSI to be  $(1^-)$  with weak-prolate deformation, and  $I^\pi$  of the HSI to be  $(4^-)$  with spherical shape + very low  $E(\text{HSI})$  or with weak-prolate deformation.

### B. Nuclear structure of low-lying states in $^{140}\text{Xe}$

Many low-lying states in  $^{140}\text{Xe}$  are populated by the  $\beta$  decay of the g.s. and/or two isomers in  $^{140}\text{I}$ . Figure 13(a) shows the experimentally observed states which are grouped from the viewpoint of nuclear structure to the g.s. band (pos1),

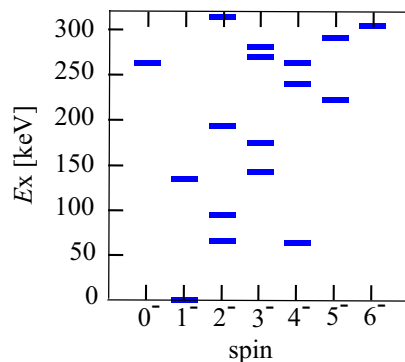


FIG. 12. Excitation energy of the low-lying states with negative parity in  $^{140}\text{I}$  vs spin calculated by the large-scale shell model.

$\gamma$  band (pos2), octupole correlated states (neg), and other states with  $E_x < 2.2$  MeV (others) in  $^{140}\text{Xe}$ . These states are compared to theoretical calculations, as shown in Figs. 13(b) and 13(c). In Fig. 13(b), theoretical states calculated by the large-scale shell model are shown. These states are classified into positive-parity bands (pos1 and pos2), which consist of states with the similar occupation numbers of valence protons and valence neutrons in each single-particle orbital, octupole  $3^-$  and  $5^-$  states (neg1), and other positive- and negative-parity states (pos and neg, respectively, in others). To calculate negative-parity octupole-correlated states in this shell model, one octupole phonon representing the octupole vibration is introduced on the shell-model states which are obtained within the valence nucleon space, as mentioned in Sec. IV A. In Fig. 13(c), theoretical states calculated in the framework of the deformed Skyrme HFB plus deformed QRPA with SkM\* Skyrme interaction [39,40] are displayed. States at  $K^\pi = 0^+$  ( $\beta$  vibrational), at  $K^\pi = 2^+$  ( $\gamma$  vibrational), and at  $K^\pi = 0^-, 1^-, 2^-$  (octupole vibrational) are calculated in this work.

The octupole band was reported in  $^{140}\text{Xe}$  for the states with spins of  $3^-(17)$  [27]. The  $\gamma$  band was identified for the band built on the  $3^+$  level at 1305 keV [5,12], while this band and the band built on the 2283-keV level were proposed as the  $s = -1$  octupole band in Ref. [11]. However, the latest discussion in Ref. [12] supported the assignment of the  $\gamma$  band. In this work, based on this result, the  $3^+$  and  $5^+$  states are discussed as the members in the  $\gamma$  band.

#### 1. Ground-state band in $^{140}\text{Xe}$

Experimental ground-state band members of  $2_1^+$ ,  $4_1^+$ , and  $6_1^+$  states at 377, 834, and 1417 keV, respectively, in  $^{140}\text{Xe}$  are shown as pos1 in Fig. 13(a). The ratio of the excitation energy for the  $2_1^+$  and  $4_1^+$  states,  $\{E(4_1^+)/E(2_1^+)\}$ , is 2.2, which is a typical value for vibrational mode. These  $E(2_1^+)$  and  $E(4_1^+)$  in  $N = 86$  isotones,  $^{140}\text{Xe}$ ,  $^{142}\text{Ba}$  [41], and  $^{144}\text{Ce}$  [42] with  $Z = 54, 56,$  and  $58$ , respectively, are plotted in Fig. 14. The  $E(4_1^+)/E(2_1^+)$  values for  $^{142}\text{Ba}$  and  $^{144}\text{Ce}$  are 2.3 and 2.4, respectively. This vibrational nature in  $N = 86$  isotones is considered to be caused by four valence neutrons together with the varying valence protons of 4, 6, and 8 against the doubly-magic core of  $^{132}\text{Sn}$  ( $Z = 50$  and  $N = 82$ ). These  $N = 86$  nuclei are suggested to be located in the transitional region where the prolate collectivity increases as proton and neutron numbers increase.

The experimental  $2_1^+$ ,  $4_1^+$ , and  $6_1^+$  levels [pos1 in Fig. 13(a)] in  $^{140}\text{Xe}$  are well reproduced in energy by the large-scale shell model [pos1 in Fig. 13(b)]. The theoretical  $E(4_1^+)/E(2_1^+)$  value is obtained to be 2.5, which is slightly larger than the experimental one. One can assume that it rather suggests an unharmonic vibrational mode is extracted by the increase of configuration mixing. In the shell-model calculation for the members in the g.s. band, an occupation number of four valence neutrons widely distribute to the  $2f_{7/2}$  orbital (about three valence neutrons) and to  $3p_{3/2}$ ,  $3p_{1/2}$ ,  $1h_{9/2}$ ,  $2f_{5/2}$ , and  $1i_{13/2}$  orbitals (total of about one).

Small-quadrupole deformation in  $^{140}\text{Xe}$  was reported with quadrupole-deformation parameter  $\beta_2$  of 0.146(3) which was

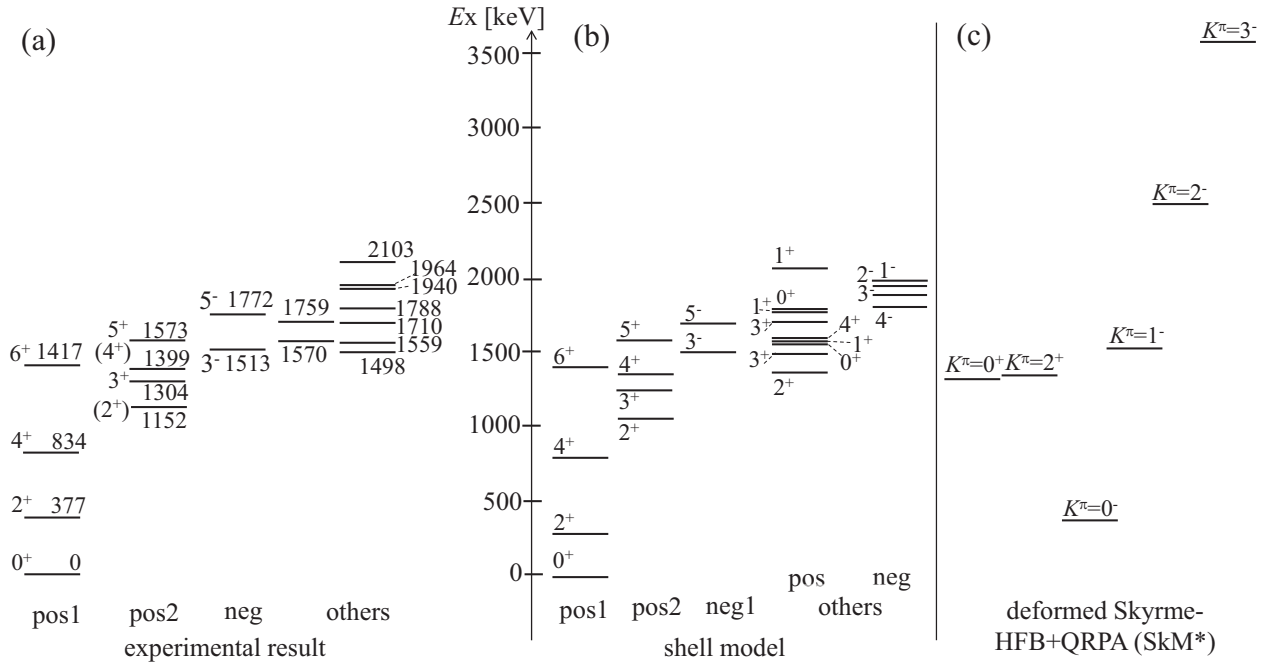


FIG. 13. (a) Experimental low-lying states with  $E_x < 2.2$  MeV in  $^{140}\text{Xe}$  grouped from the viewpoint of nuclear structure. Theoretical levels are calculated in (b) the large-scale shell model and by (c) the deformed Skyrme-HFB + QRPA (SkM\*).

experimentally determined by the lifetime measurement of the  $2_1^+$  level in Ref. [16]. This result was supported by the  $B(E2; 0_1^+ \rightarrow 2_1^+)$  value obtained by the Coulomb-excitation experiment in Ref. [17]. A slightly smaller  $\beta_2$  value of 0.102 is theoretically obtained by the deformed-HFB calculation in good agreement with the experimental results.

## 2. $\gamma$ band in $^{140}\text{Xe}$

The  $3^+$  and  $5^+$  states at 1304 and 1573 keV, respectively, were reported to be members of the  $\gamma$  band in Refs. [5,12]. A candidate for the  $4^+$  member could be suggested to be the newly found state at 1399 keV, because it is located at  $E(3^+) < E_x < E(5^+)$ . Additionally, the spin of this state is supposed to be higher than 2, because this state is populated by the  $\beta$  decay of the HSI with relatively large  $\beta$ -decay intensity. A

candidate of the  $2^+$  member in the  $\gamma$  band could be suggested to be the newly found state at 1152 keV, because this state is located at  $E_x < E(3^+)$ . And also the assignment of  $2^+$  is supported by the two depopulating transitions of 775 keV ( $\rightarrow 2_1^+$  level at 377 keV) and 1151 keV ( $\rightarrow$  g.s.). Positive-parity states [pos2 in Fig. 13(a)] are displayed as the  $\gamma$ -band members including candidates of ( $2_2^+$ ) and ( $4_2^+$ ) states.

These  $\gamma$ -vibrational ( $\gamma$ -soft) structures in the (quasi-) $\gamma$  band of  $^{140}\text{Xe}$  are discussed by using the Davydov model [43], even though this is the model based on fixed stable  $\gamma$  asymmetry (triaxiality). The  $\gamma$ -deformation parameter is experimentally estimated to be  $\approx 22^\circ$  from the ratio of the  $E_x$  of the first and the second  $2^+$  states  $\{E(2_2^+)/E(2_1^+)\}$  of 3.06. This may suggest large- $\gamma$  collectivity in the low-lying states of  $^{140}\text{Xe}$ .

Four experimental (quasi-) $\gamma$ -band members with spin of 2–5 are well reproduced in energy by the large-scale shell-model calculation [pos2 in Fig. 13(b)]. Large configuration mixing is found in the theoretical result for these states with occupation number of four valence neutrons which widely distribute to the  $2f_{7/2}$  orbital ( $\approx 2.7$  valence neutrons) and to the  $3p_{3/2}$ ,  $3p_{1/2}$ ,  $1h_{9/2}$ ,  $2f_{5/2}$ , and  $1i_{13/2}$  orbitals (total  $\approx 1.3$ ). As this wider distribution in the states (pos2) than those in the states (pos1) suggests that the states (pos2) could have larger collectivity, the states (pos2) could be expected to have vibrational-like structure. By applying the Davydov model to these theoretical states (pos2), the  $\gamma$ -deformation parameter is obtained to be  $\approx 21^\circ$  from the theoretical  $E(2_2^+)/E(2_1^+)$  of 3.34. As these positive-parity states are deduced by the shell-model calculation without octupole correlation, these states could be supported to have a  $\gamma$ -vibrational ( $\gamma$ -soft) structure rather than to be members in the  $s = -1$  octupole

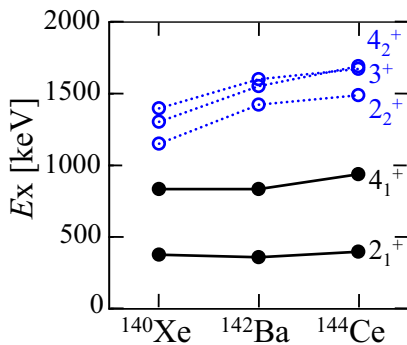


FIG. 14. Systematics of experimental excitation energy for the positive-parity states with spin of 2–4 in  $N = 86$  isotopes, Xe (in this work), Ba [41], and Ce [42].

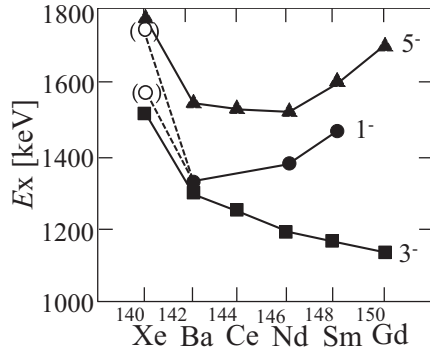


FIG. 15. Systematics of excitation energy of octupole collective  $1^-$ ,  $3^-$ , and  $5^-$  states in  $N = 86$  isotones. Data for Xe and others are taken from this work and Refs. [41,42,46–48].

band. A possible candidate of the  $2^+$  state at 1152 keV as the  $2^+$  member in the (quasi-) $\gamma$  band is well reproduced by the calculated  $K^\pi = 2^+$  state in the deformed Skyrme-HFB + QRPA (SkM\*), as shown in Fig. 13(c).

$\gamma$ -band members were reported in other  $N = 86$  isotones, Ba [41] and Ce [42] with  $Z = 56$  and  $58$ , respectively. Figure 14 shows experimentally obtained  $E_x$  of the  $2_2^+$ ,  $3^+$ , and  $4_2^+$  states corresponding the (quasi-) $\gamma$  band in the  $N = 86$  isotones including  $^{140}\text{Xe}$ . By applying the Davydov model,  $\gamma$ -deformation parameters are extracted to be  $19^\circ$  and  $20^\circ$  from the ratio of  $E(2_2^+)/E(2_1^+)$  for  $^{142}\text{Ba}$  and  $^{144}\text{Ce}$ , respectively, which indicates larger- $\gamma$  collectivity in the  $N = 86$  isotones. The  $E_x$  of the  $2_2^+$ ,  $3^+$ , and  $4_2^+$  states in the (quasi-) $\gamma$  band increase as a function of proton number; however, the energy difference between the  $3^+$  and  $4_2^+$  states decreases and mostly degenerates for  $^{144}\text{Ce}$ . This degeneracy is typical nature of the  $\gamma$ -unstable rotor, which is known as the Willets-Jean model [44,45]. This may suggest the increase of  $\gamma$  softness with the increase of the proton number in  $N = 86$  isotones.

### 3. Octupole-collective states and other states in $^{140}\text{Xe}$

The experimental  $3^-$  and  $5^-$  states at 1513 and 1772 keV, respectively [neg in Fig. 13(a)], were reported as members of the octupole band in  $^{140}\text{Xe}$  [4,11,16]. In the high-spin region of  $I > 12$ , reported interleaved positive- and negative-parity states were explained as members of the octupole-rotational bands with linearity for plots of  $E_x$  vs  $I(I + 1)$ . However the  $E_x$  of the  $3^-$  and  $5^-$  states are out of this linearity, which is supposed to be caused by octupole-vibrational nature. The  $E_x$  of the  $3^-$  and the  $5^-$  states in  $^{140}\text{Xe}$  are shown in Fig. 15, comparing to the  $E_x$  of the  $1^-$  (closed circle),  $3^-$  (closed square), and  $5^-$  (closed triangle) states in  $N = 86$  isotones,  $^{142}\text{Ba}$  [41],  $^{144}\text{Ce}$  [42],  $^{146}\text{Nd}$  [46],  $^{148}\text{Sm}$  [47], and  $^{150}\text{Gd}$  [48] with  $Z = 56, 58, 60, 62,$  and  $64$ , respectively. The  $E_x$  of the  $3^-$  and  $5^-$  states in  $^{140}\text{Xe}$  are higher than those in  $^{142}\text{Ba}$  isotope. This may suggest weaker octupole  $Y_{30}$  collectivity in  $^{140}\text{Xe}$  comparing to that in  $^{142}\text{Ba}$ . This  $^{142}\text{Ba}$  nucleus has two neutrons less than  $^{144}\text{Ba}$  with  $Z = 56$  and  $N = 88$ , which is expected to have the largest octupole collectivity in this mass region [1].

The  $E_x$  of the  $1^-$  states are systematically found to be higher than those of the  $3^-$  states in  $N = 86$  isotones, as shown in Fig. 15. The  $1^-$  states are supposed to be assigned as a  $K^\pi = 1^-$  state and not as a member of the  $K^\pi = 0^-$  rotational band. In  $^{140}\text{Xe}$ , the  $1^-$  state was not yet reported. Many experimental low-lying states with  $E_x < 2.2$  MeV [others in Fig. 13(a)] are populated in the  $\beta$  decay of the g.s. and two isomers in  $^{140}\text{I}$ . Two states at 1570 and 1759 keV are depopulated by two transitions of 1194 keV ( $\rightarrow 2_1^+$ ) and 1570 keV ( $\rightarrow$  g.s.) and of 1382 keV ( $\rightarrow 2_1^+$ ) and 1759 keV ( $\rightarrow$  g.s.), respectively. This suggests that  $I^\pi$  of these states may be assigned as  $1^+$ ,  $1^-$ , and  $2^+$ . One of these states is supposed to be a possible candidate of the  $1^-$  state. The experimental  $E_x$  of both possible candidates are plotted by open circles in Fig. 15. Both  $E_x$  are higher and lower than those of the  $3^-$  and the  $5^-$  states, respectively, even though it cannot be concluded which is the  $1^-$  state.

Experimental negative-parity states are compared with the large-scale shell-model calculation [neg1 and neg-others in Fig. 13(b)] including the octupole-phonon ( $f$  boson) excitations based on the shell-model states. Single  $f$ -boson energy is introduced to reproduce the experimental ( $3^-$ ) state at 1513 keV. The experimental  $5^-$  state is well reproduced in energy by the shell-model calculation as one of the quintet of ( $f$  boson  $3^-$ )  $\otimes$  (shell-model  $2^+$ ). Other  $1^- - 4^-$  members of the quintet are shown as neg-other in Fig. 13(b). Theoretical positive-parity other states are displayed as pos-other in this figure. As theoretical  $E_x$  of the  $1^+$  and the  $1^-$  states is higher than  $E_x$  of the  $3^-$  state, the experimental states at 1570 and 1759 keV may be possible candidates for these  $1^-$  and  $1^+$  states.

Experimental negative-parity states are also compared with the deformed Skyrme-HFB + QRPA (SkM\*) calculation. Theoretical  $E_x$  of the intrinsic octupole quadruplet states with  $K^\pi = 0^-, 1^-, 2^-,$  and  $3^-$  in  $^{140}\text{Xe}$  are shown in Fig. 13(c). The  $E_x$  of candidates for the  $1^-$  states at 1570 and 1759 keV are supported by the theoretical  $E_x$  of 1.53 MeV for the  $K^\pi = 1^-$  state. Experimental  $E_x$  for the  $K^\pi = 0^-$  state can be estimated to be 1.77 MeV assuming linear behavior of  $E_x$  vs  $I(I + 1)$  in the spin region of  $I > 12$  for the reported interleaved positive- and negative-parity rotational bands [4,11,16]. This experimentally estimated  $E_x$  is much higher than the theoretical  $E_x$  of 0.38 MeV for the  $K^\pi = 0^-$  state. This model is based on the weak-prolate deformation coupled to octupole vibration. This energy discrepancy may be caused by other conditions, such as nuclear shape with weak-prolate coupled to small-octupole deformation, or with weak-triaxial coupled to octupole vibration, and so on. The theoretical  $E_x$  of the  $K^\pi = 2^-$  state is calculated to be 2.45 MeV, as shown in Fig. 13(c). Experimentally observed states at  $E_x \approx 2.5$  MeV are expected to contain the candidate of the  $K^\pi = 2^-$  state. Some states are deexcited by transitions which populate the octupole correlated  $3^-$  state at 1513 keV and/or one of the candidates for the  $1^-$  state at 1570 keV.

## V. SUMMARY

Shape coexistence and shape transition are expected to appear in transitional nuclei with  $Z > 50$  and  $N > 82$ . Nuclear

structure for one of the neutron-rich nuclei in this mass region,  $^{140}\text{Xe}$  ( $Z = 54$  and  $N = 86$ ), is studied by the  $\beta$  decay of  $^{140}\text{I}$ . The experiment is carried out in the EURICA decay-spectroscopy project at RIBF, RIKEN. The neutron-rich  $^{140}\text{I}$  nucleus is produced by two reactions of the direct in-flight fission of a U beam at a primary target and of the  $\beta$  decay of  $^{140}\text{Te}$  at the active catcher, WAS3ABi. In this work, two  $\beta$ -decay isomers in the odd-odd nucleus  $^{140}\text{I}$  are newly found and decay schemes are constructed for the  $\beta$  decay of the HSI and for the mixed  $\beta$  decays of the g.s. and the LSI. Low-lying states in  $^{140}\text{I}$  and  $^{140}\text{Xe}$  are discussed, comparing theoretical calculations in the large-scale shell model and in the deformed Skyrme-HFB + QRPA (SkM\*).

$I^\pi$  of the g.s., the LSI, and the HSI in  $^{140}\text{I}$  are experimentally proposed to be  $(2^-, 3^-, 3^+)$ ,  $(0^-, 1^-, 1^+)$ , and  $(4^-, 5^-, 5^+)$ , respectively. Additionally, from systematical estimation of  $I^\pi$  as a coupling of the 53rd valence proton and the 87th valence neutron, candidates for  $I^\pi$  for the g.s., the LSI, and the HSI are deduced to be  $(2^-, 3^-)$ ,  $(0^-, 1^-)$ , and  $(4^-, 5^-)$ , respectively, with spherical shape. In the case of weak-prolate deformation, candidates for  $I^\pi$  are proposed to be  $(1^-)$  and  $(4^-)$  for the LSI and the HSI, respectively. Finally, comparing to the shell-model calculation and considering the experimental transition probability between the g.s. and the isomers,  $I^\pi$  are presumed to be  $(2^-)$  with spherical shape for the g.s.,  $(1^-)$  with weak-prolate deformation for the LSI, and  $(4^-)$  with spherical shape plus very low  $E_x(\text{HSI})$  or with weak-prolate deformation for the HSI.

Various nuclear structures are observed in the low-lying states of  $^{140}\text{Xe}$ . The ground-state band can be explained as a typical vibrational mode from the  $E(4_1^+)/E(2_1^+)$  of 2.2. The excitation energy of these band members are reproduced in energy by the shell-model calculation with large configuration mixing with spread of occupation number of four valence-neutron particles.

Possible candidates for (quasi-) $\gamma$  band members of  $2^+$  and  $4^+$  are proposed. These (quasi-) $\gamma$  band members at  $2^+_{-5^+}$  are well reproduced in energy by the shell-model calculation with larger-configuration mixing than that for the ground-state band members. This candidate of the  $2^+$  state is supported by the  $K^\pi = 2^+$  state in the deformed

Skyrme-HFB + QRPA calculation. Applying the Davydov model, a large  $\gamma$ -deformation parameter is extracted to be  $\approx 22^\circ$  by using the experimental  $E(2_2^+)/E(2_1^+) = 3.06$ . Comparing the experimental excitation-energy difference between the  $3^+$  and the  $4^+$  states in  $N = 86$  isotones, an increase of  $\gamma$  softness can be seen with the increase of proton number.

Experimental  $E_x$  of the  $3^-$  and the  $5^-$  octupole-band members in  $^{140}\text{Xe}$  are higher than those in  $^{142}\text{Ba}$ . This may suggest weaker-octupole  $Y_{30}$  collectivity in  $^{140}\text{Xe}$  ( $Z = 54$ ) than that in  $^{142}\text{Ba}$  ( $Z = 56$ ), because the nucleus  $^{144}\text{Ba}$  ( $Z = 56$  and  $N = 88$ ) is known to have the largest-octupole collectivity in this mass region. Possible candidate of the  $1^-$  state, which could be explained to be the one-phonon octupole-vibrational state with  $K^\pi = 1^-$ , is proposed to be states at 1570 or 1750 keV. These candidates are supported by the theoretical calculations in the large-scale shell model including the octupole phonon and by the deformed Skyrme-HFB + QRPA.

This work demonstrates that in the low-lying states of  $^{140}\text{Xe}$ , coexistence of nuclear structures, such as vibrational nature with prolate collectivity, large- $\gamma$  collectivity ( $\gamma$  softness), and octupole-vibrational nature, could appear due to four valence protons and four valence neutrons being coupled to the doubly-magic nucleus  $^{132}\text{Sn}$ .

#### ACKNOWLEDGMENTS

The authors are grateful to the RIBF staffs in RIKEN for providing beams. The authors acknowledge the Euroball Owners Committee for the loan of Ge detectors and the Pre-Spec Collaboration for the use of the readout electronics. Part of the WAS3ABi was supported by the Rare Isotope Science Project which is funded by the Ministry of Education, Science, and Technology (MEST) and National Research Foundation (NRF) of Korea (2013M7A1A1075764). Support by IN2P3-LIA agreements is also acknowledged. C.B.M. acknowledges the support from Institute for Basic Science in Republic of Korea (Grant No. IBS-R031-D1). B.M. acknowledges the support from Institute for Basic Science in Republic of Korea (Grant No. IBS-R031-Y1).

[1] B. Bucher, S. Zhu, C. Y. Wu, R. V. F. Janssens, D. Cline, A. B. Hayes, M. Albers, A. D. Ayangeakaa, P. A. Butler, C. M. Campbell, M. P. Carpenter, C. J. Chiara, J. A. Clark, H. L. Crawford, M. Cromaz, H. M. David, C. Dickerson, E. T. Gregor, J. Harker, C. R. Hoffman, B. P. Kay, F. G. Kondev, A. Korichi, T. Lauritsen, A. O. Macchiavelli, R. C. Pardo, A. Richard, M. A. Riley, G. Savard, M. Scheck, D. Seweryniak, M. K. Smith, R. Vondrasek, and A. Wiens, *Phys. Rev. Lett.* **116**, 112503 (2016).

[2] B. Bucher, S. Zhu, C. Y. Wu, R. V. F. Janssens, R. N. Bernard, L. M. Robledo, T. R. Rodríguez, D. Cline, A. B. Hayes, A. D. Ayangeakaa, M. Q. Buckner, C. M. Campbell, M. P. Carpenter, J. A. Clark, H. L. Crawford, H. M. David, C. Dickerson, J. Harker, C. R. Hoffman, B. P. Kay, F. G. Kondev,

T. Lauritsen, A. O. Macchiavelli, R. C. Pardo, G. Savard, D. Seweryniak, and R. Vondrasek, *Phys. Rev. Lett.* **118**, 152504 (2017).

[3] M. Bentalab, N. Schulz, E. Lubkiewicz, J. L. Durell, C. J. Pearson, W. R. Phillips, J. Shannon, B. J. Varley, I. Ahmad, C. J. Lister *et al.*, *Z. Phys. A* **354**, 143 (1996).

[4] W. Urban, T. Rząca-Urban, N. Schulz, J. L. Durell, W. R. Phillips, A. G. Smith, B. J. Varley, and I. Ahmad, *Eur. Phys. J. A* **16**, 303 (2003).

[5] W. Urban, K. Sieja, T. Rząca-Urban, M. Czerwiński, H. Naïdja, F. Nowacki, A. G. Smith, and I. Ahmad, *Phys. Rev. C* **93**, 034326 (2016).

[6] E. Cheifetz, J. B. Wilhelmy, R. C. Jared, and S. G. Thompson, *Phys. Rev. C* **4**, 1913 (1971).

- [7] A. Wolf and E. Cheifetz, *Phys. Rev. C* **13**, 1952 (1976).
- [8] S. Zhu, X. Zhao, J. H. Hamilton, A. V. Ramayya, Q. Lu, W.-C. Ma, L. K. Peker, J. Kormicki, H. Xie, W. B. Gao *et al.*, *Rev. Mex. Fis.* **38**, 53 (1992).
- [9] K. Butler-Moore, J. H. Hamilton, A. V. Ramayya, S. Zhu, X. Zhao, W. C. Ma, J. Kormicki, J. K. Deng, W. B. Gao, J. D. Cole *et al.*, *J. Phys. G: Nucl. Part. Phys.* **19**, L121 (1993).
- [10] J. H. Hamilton, A. V. Ramayya, J. K. Hwang, J. Kormicki, B. R. S. Babu, A. Sandulescu, A. Florescu, W. Greiner, G. M. Ter-Akopian, Yu. Ts. Oganessian *et al.*, *Prog. Part. Nucl. Phys.* **38**, 273 (1997).
- [11] Y. Huang, S. J. Zhu, J. H. Hamilton, E. H. Wang, A. V. Ramayya, Z. G. Xiao, H. J. Li, Y. X. Luo, J. O. Rasmussen, G. M. Ter-Akopian, and Y. T. Oganessian, *Phys. Rev. C* **93**, 064321 (2016).
- [12] H. Naidja, F. Nowacki, B. Bounthong, M. Czerwiński, T. Rząca-Urban, T. Rogiński, W. Urban, J. Wiśniewski, K. Sieja, A. G. Smith, J. F. Smith, G. S. Simpson, I. Ahmad, and J. P. Greene, *Phys. Rev. C* **95**, 064303 (2017).
- [13] C. Goodin, J. R. Stone, N. J. Stone, A. V. Ramayya, A. V. Daniel, J. H. Hamilton, K. Li, J. K. Hwang, G. M. Ter-Akopian, and J. O. Rasmussen, *Phys. Rev. C* **79**, 034316 (2009).
- [14] S. Mukhopadhyay, L. S. Danu, D. C. Biswas, A. Goswami, P. N. Prashanth, L. A. Kinage, A. Chatterjee, and R. K. Choudhury, *Phys. Rev. C* **85**, 064321 (2012).
- [15] S. Ilieva, T. Kröll, J.-M. Régis, N. Saed-Samii, A. Blanc, A. M. Bruce, L. M. Fraile, G. de France, A.-L. Hartig, C. Henrich, A. Ignatov, M. Jentschel, J. Jolie, W. Korten, U. Koster, S. Lalkovski, R. Lozeva, H. Mach, N. Marginean, P. Mutti, V. Pazy, P. H. Regan, G. S. Simpson, T. Soldner, M. Thurauf, C. A. Ur, W. Urban, and N. Warr, *Phys. Rev. C* **94**, 034302 (2016).
- [16] A. Lindroth, B. Fogelberg, H. Mach, M. Sanchez-Vega, and J. Bielčík, *Phys. Rev. Lett.* **82**, 4783 (1999).
- [17] Th. Kröll, T. Behrens, R. Krücken, V. Bildstein, R. Gernhäuser, P. Maierbeck, I. Stefanescu, O. Ivanov, J. Van de Walle, N. Warr *et al.*, *Eur. Phys. J. Spec. Top.* **150**, 127 (2007).
- [18] S. Nishimura, *Prog. Theor. Exp. Phys.* **2012**, 03C006 (2012).
- [19] P.-A. Söderström, S. Nishimura, P. Doornenbal, G. Lorusso, T. Sumikama, H. Watanabe, Z. Y. Xu, H. Baba, F. Browne, S. Go *et al.*, *Nucl. Instrum. Methods Phys. Res. Sect. B* **317**, 649 (2013).
- [20] T. Kubo, D. Kameda, H. Suzuki, N. Fukuda, H. Takeda, Y. Yanagisawa, M. Ohtake, K. Kusaka, K. Yoshida, N. Inabe *et al.*, *Prog. Theor. Exp. Phys.* **2012**, 03C003 (2012).
- [21] J. Allison, K. Amako, J. Apostolakis, P. Arce, M. Asai, T. Aso, E. Bagli, A. Bagulya, S. Banerjee, G. Barrand *et al.*, *Nucl. Instrum. Methods Phys. Res. Sect. A* **835**, 186 (2016), and references therein, <http://geant4.web.cern.ch/>.
- [22] P. Lee, C.-B. Moon, C. S. Lee, A. Odahara, R. Lozeva, A. Yagi, S. Nishimura, P. Doornenbal, G. Lorusso, P.-A. Söderström, T. Sumikama, H. Watanabe, T. Isobe, H. Baba, H. Sakurai, F. Browne, R. Daido, Y. Fang, H. Nishibata, Z. Patel, S. Rice, L. Sinclair, J. Wu, Z. Y. Xu, R. Yokoyama, T. Kubo, N. Inabe, H. Suzuki, N. Fukuda, D. Kameda, H. Takeda, D. S. Ahn, D. Murai, F. L. Bello Garrote, J. M. Daugas, F. Didierjean, E. Ideguchi, T. Ishigaki, H. S. Jung, T. Komatsubara, Y. K. Kwon, S. Morimoto, M. Niikura, I. Nishizuka, and K. Tshoo, *Phys. Rev. C* **92**, 044320 (2015).
- [23] J. Wu, S. Nishimura, P. Möller, M. R. Mumpower, R. Lozeva, C. B. Moon, A. Odahara, H. Baba, F. Browne, R. Daido *et al.*, *Phys. Rev. C* **101**, 042801(R) (2020).
- [24] B. Moon, C.-B. Moon, A. Odahara, R. Lozeva, P.-A. Söderström, F. Browne, C. Yuan, A. Yagi, B. Hong, H. S. Jung, P. Lee, C. S. Lee, S. Nishimura, P. Doornenbal, G. Lorusso, T. Sumikama, H. Watanabe, I. Kojouharov, T. Isobe, H. Baba, H. Sakurai, R. Daido, Y. Fang, H. Nishibata, Z. Patel, S. Rice, L. Sinclair, J. Wu, Z. Y. Xu, R. Yokoyama, T. Kubo, N. Inabe, H. Suzuki, N. Fukuda, D. Kameda, H. Takeda, D. S. Ahn, Y. Shimizu, D. Murai, F. L. Bello Garrote, J. M. Daugas, F. Didierjean, E. Ideguchi, T. Ishigaki, S. Morimoto, M. Niikura, I. Nishizuka, T. Komatsubara, Y. K. Kwon, and K. Tshoo, *Phys. Rev. C* **96**, 014325 (2017).
- [25] E. Lund and G. Rudstam, *Phys. Rev. C* **13**, 1544 (1976).
- [26] H. Ahrens, P. Patzelt, and G. Herrmann, *J. Inorg. Nucl. Chem.* **38**, 191 (1976).
- [27] N. Nica, *Nucl. Data Sheets* **154**, 1 (2018).
- [28] M. Wang, W. J. Huang, F. G. Kondev, G. Audi, and S. Naimi, *Chin. Phys. C* **45**, 030003 (2021).
- [29] F. G. Kondev, M. Wang, W. J. Huang, S. Naimi, and G. Audi, *Chin. Phys. C* **45**, 030001 (2021).
- [30] D. Otero, A. N. Proto, E. Duering, and M. L. Pérez, *Phys. Rev. C* **23**, 2691 (1981).
- [31] W. Urban, M. Saha Sarkar, S. Sarkar, T. Rząca-Urban, J. L. Durell, A. G. Smith, J. A. Genevey, J. A. Pinston, G. S. Simpson, and I. Ahmad, *Eur. Phys. J. A* **27**, 257 (2006).
- [32] T. Rząca-Urban, K. Pałowska, W. Urban, A. Ziłomaniec, J. Genevey, J. A. Pinston, G. S. Simpson, M. Saha Sarkar, S. Sarkar, H. Faust, A. Scherillo, I. Tsekhanovich, R. Orlandi, J. L. Durell, A. G. Smith, and I. Ahmand, *Phys. Rev. C* **75**, 054319 (2007).
- [33] P. K. Joshi, B. Singh, S. Singh, and A. K. Jain, *Nucl. Data Sheets* **138**, 1 (2016).
- [34] N. Nica, *Nucl. Data Sheets* **122**, 1 (2014).
- [35] E. Teruya, N. Yoshinaga, K. Higashiyama, and A. Odahara, *Phys. Rev. C* **92**, 034320 (2015).
- [36] N. Yoshinaga, K. Yanase, C. Watanabe, and K. Higashiyama, *Prog. Theor. Exp. Phys.* **2021**, 063D01 (2021).
- [37] E. Teruya, K. Higashiyama, and N. Yoshinaga, *Phys. Rev. C* **93**, 064327 (2016).
- [38] K. Yanase, E. Teruya, K. Higashiyama, and N. Yoshinaga, *Phys. Rev. C* **98**, 014308 (2018).
- [39] K. Yoshida and T. Nakatsukasa, *Phys. Rev. C* **88**, 034309 (2013).
- [40] K. Yoshida and N. V. Giai, *Phys. Rev. C* **78**, 014305 (2008).
- [41] T. D. Johnson, D. Symochko, M. Fadil, and J. K. Tuli, *Nucl. Data Sheets* **112**, 1949 (2011).
- [42] A. A. Sonzogni, *Nucl. Data Sheets* **93**, 599 (2001).
- [43] A. S. Davydov and G. F. Filippov, *Nucl. Phys.* **8**, 237 (1958).
- [44] L. Willets and M. Jean, *Phys. Rev.* **102**, 788 (1956).
- [45] R. F. Casten, in *Nuclear Structure from a Simple Perspective*, edited by P. E. Hodgson (Oxford University Press, New York, 1990).
- [46] Yu. Khazov, A. Rodionov, and G. Shulyak, *Nucl. Data Sheets* **136**, 163 (2016).
- [47] N. Nica, *Nucl. Data Sheets* **117**, 1 (2014).
- [48] S. K. Basu and A. A. Sonzogni, *Nucl. Data Sheets* **114**, 435 (2013).